UiT The Arctic University of Norway

Faculty of Biosciences, Fisheries and Economics, Department of Arctic and Marine Biology

Seasonal Variations in Vertical Flux of particulate matter and composition in the Northern Barents Sea

Tassawer Hussain Master's thesis in Biology, BIO-3950, Nov 2023

Seasonal Variations in Vertical Flux of particulate matter and compositions in the Northern Barents Sea

Tassawer Hussain

Arctic Marine Ecology

Submission date: November 15, 2023

Supervisor: Professor Marit Reigstad[1]

Co-supervisor 1: Yasemin V. Bodur[1]

Co-supervisor 2: Griselda Anglada Ortiz[1]

[1]The Arctic University of Norway

The Arctic University of Norway UiT

Department of Arctic and Marine Ecology

Acknowledgements

This master thesis was the part of Nansen Legacy project funded by the Research Council of Norway and Norwegian Ministry of Education and Research. It was supervised by Professor Marit Reigstad from the Arctic University of Norway (UiT) and co-supervised by Yasemin V. Bodur and Griselda Anglada Ortiz from the Arctic University of Norway (UiT).

First and foremost, I extend my deepest appreciation to my main supervisor, Professor Marit Reigstad, whose expertise, guidance, and unwavering support have been invaluable throughout the research process. Professor Reigstad's insightful feedback and encouragement have significantly shaped the development of this thesis. I am also grateful to my co-supervisors, Yasemin V. Bodur and Griselda Anglada Ortiz, for their constructive feedback, scholarly insights, and commitment to enhancing the quality of my work. Their collective guidance has been instrumental in refining the scope and depth of my research.

A special thanks go to Bilal Afzal and Mohsin Khan whose technical, interesting discussions, emotional and moral support provided me with strength and encouragement during challenging phases of this academic endeavor.

Lastly, I would like to express my gratitude to my family and friends for their unwavering encouragement and understanding throughout this academic journey. Your support has been a constant source of inspiration, and I am truly fortunate to have such a strong support system.

Thank you to everyone who played a role, in the completion of this thesis. Your contributions have been integral to its success.

Sincerely, Tassawer Hussain, Tromsø, November 2023

Abstract

The Barents Sea is an inflow shelf sea in the Arctic Ocean which experiences climate change consequently reduction in the sea ice extent thereby significantly impacting its ecological importance. This study investigates seasonal variations in the vertical flux of particulate matter including both particulate organic matter (chl a) and particulate inorganic matterin the form of $CaCO_3$ contributed by planktonic marine calcifiers, and explores the implications of seasonality on the vertical flux of particulate matter (TPM) and composition (PIM and POM). Long term sediment traps were deployed at the Nansen Legacy M1 mooring station (79°34.975N; 28°04.38E) during 2019-2020. The study parameters include total particulate matter (organic and inorganic matter), chlorophyll a, and role of planktonic marine calcifiers (foraminifers and pteropods). The annual vertical flux of TPM has been found ~5.96 g m^{-2} $year^{-1}$. The PIM contributes ~ 4.29 g m^{-2} $year^{-1}$ and POM contributes ~1.67 g m^{-2} $year^{-1}$ to the TPM. The annual vertical flux of chl a has been found ~ 0.16 g m^{-2} $year^{-1}$ and calcifiers contribute ~ 0.42 g m^{-2} $year^{-1}$ to PIM as $CaCO_3$. Notably, the total particulate matter flux exhibited peaks during polar night, particularly in December, with dominant contributions from particulate inorganic matter during winter, contrasting with higher particulate organic matter flux in productive and summer periods. Chlorophyll a demonstrated unexpected high flux during December, suggesting aged and degraded organic materials influenced by water advection and resuspension processes as supported by low chlorophyll a/phaeo-pigments ratios. Seasonal trends in the contribution of planktonic marine calcifiers highlighted lower fluxes during winter and higher contributions during summer, showcasing varying deposition patterns and shell sizes among different species. This study emphasizes the connections between environmental conditions, seasonal changes, and $CaCO_3$ flux to the vertical flux of total particulate matter in the Barents Sea, and offering key insights for future exploration of its seasonal dynamics.

Key words:

Arctic Ocean, Barents Sea, chlorophyll a, environmental dynamics, marine calcifiers, seasonal variations, total particulate matter, and vertical flux.

Table of Contents

List of Tables

List of Figures

1 Introduction

The Arctic Ocean is undergoing unprecedented changes due to the progression of climate change, resulting in the loss of sea ice cover (Serreze & Meier, 2019; Walsh et al., 2011). To study the effects of climate change and global warming on the Arctic Ocean, the geographical location and hydrographical characteristics of the Barents Sea make it a region of substantial scientific interest and ecological significance and it is also seasonally ice covered as compared to the central Arctic Ocean.

1.1 Physical features of the Barents Sea

The Barents Sea is a continental shelf sea in the Arctic Ocean with maximum depth of 500m while average depth is about 230m (Loeng, 1991; Lundesgaard et al., 2022). The Barents Sea extends from 74°N to 80°N and 37°E to 50°E; north of Norway and west of Novaya Zemlya (Russia) with an area of $1.4\times10^6 km^2$ as shown in Figure 1(a,b) (Drinkwater, 2011; Dybwad et al., 2022). The bathymetry features of the Barents Sea extensive shallow areas (Spitsbergenbanken and southern parts <50m), deep troughs (Bjørnøyrenna~500m), and isolated banks (the Central Bank, the Svalbard Bank and the Great Bank) (Loeng, 1991; Wassmann et al., 2006), contributing to a dynamic underwater landscape that significantly effects the distribution and movement of water masses.

The warm and saline Atlantic Water (AW) arrives in the Barents Sea via two channels, one follows with the Norwegian coast into the central Barents Sea, eventually cooling down before reaching to the Kara Sea in the East (Carmack et al., 2006; Loeng, 1991; Loeng & Drinkwater, 2007; Sundfjord et al., 2020). The second, channel follows the continental shelf break toward the Fram Strait as the West Spitsbergen Current, subsequently splits into three branches. One branch flows west towards the Fram Strait, second branch flows north to the Yermak Plateau which later joins the third branch flowing north of the Svalbard. Here, the two branches combine to make the Fram Strait Branch of Atlantic Water (FSAW) which flows eastwards to the Franz Josef Land (Carmack et al., 2006; Loeng, 1991; Loeng & Drinkwater, 2007; Lundesgaard et al., 2022). A small fraction flows east of Svalbard via Kvitøya trough and flows south and southwest of Svalbard (Lundesgaard et al., 2022) as shown in the Figure 1b (Dybwad et al., 2022) . There, it mixes with the cold and fresher Polar Water (PW) (Sundfjord et al., 2020).

The northern Barents Sea is seasonally ice covered by and melting of ice in summer decrease the salinity and leads to fresher water on the surface and more saline water underneath, leading towards

a stronger vertical stratification (Loeng, 1991) . In this part, the PW dominates over the AW. Whereas, the southern and south-western Barents Sea is ice free throughout the year and the AW dominates in this section of the Barents Sea (Loeng, 1991).

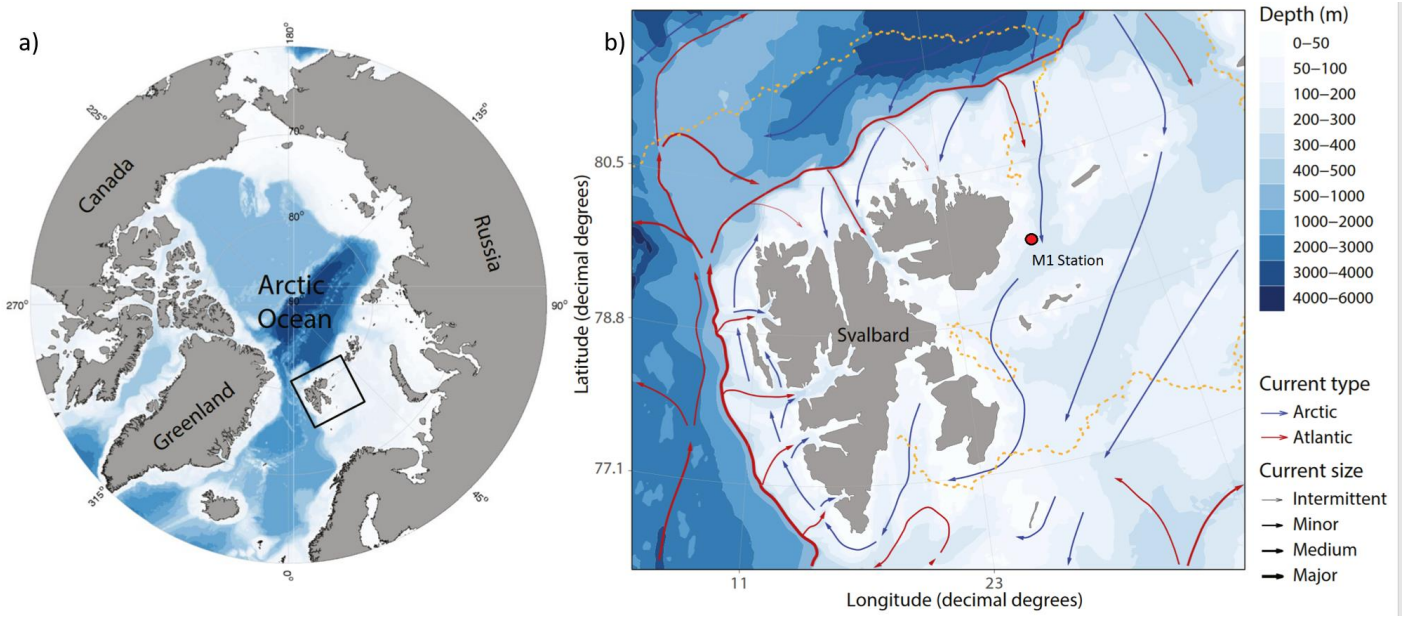

Figure 1. a) The Pan-Arctic view of the Arctic Ocean is shown where the black square represents the study area. b) The study area in the northern Barents Sea is shown, the Red Dot denotes the research station M1 and the yellow lines show the median ice edge in May 2018. (Modified from Dybwad et al. 2022)

The distribution of these waters and their layering in the vertical domain significantly impact the properties of ocean, ecology, biogeochemistry, sea ice, and atmospheric climate (Loeng, 1991; Loeng & Drinkwater, 2007). The vertical layering of water masses, with AW flowing below PW due to differences in salinity, plays a essential role in the ocean-atmosphere interactions of the region (Loeng, 1991; Lundesgaard et al., 2022). Stratification in the northern Barents Sea is seasonal and depends upon the density of the surface water. The surface water becomes more cold and saline during the winter hence, increasing the density which leads to weak stratification. Weak stratification during winter, facilitates the vertical mixing. Stratification becomes strong when the ice melts which limits the vertical mixing (Loeng, 1991). Moreover, seasonal variations, including surface warming in ice-free areas during summer, further contribute to the complexity of the water mass distribution and interactions (Lundesgaard et al., 2022).

1.2 Seasonal Variations and their Significance

The transition from cold, ice-covered winters to ice-free, productive summers significantly impacts primary production and the communities of phytoplankton (Leu et al., 2011). This seasonal

change, notably influenced by the decline in sea ice extent, leads to variations in vertical flux, particularly affecting carbon content. The interplay between ice and snow cover, the grazing community, and environmental factors significantly influences the onset, quality, and quantity of primary production that sinks into deeper waters (Lalande et al., 2014; Reigstad et al., 2008).

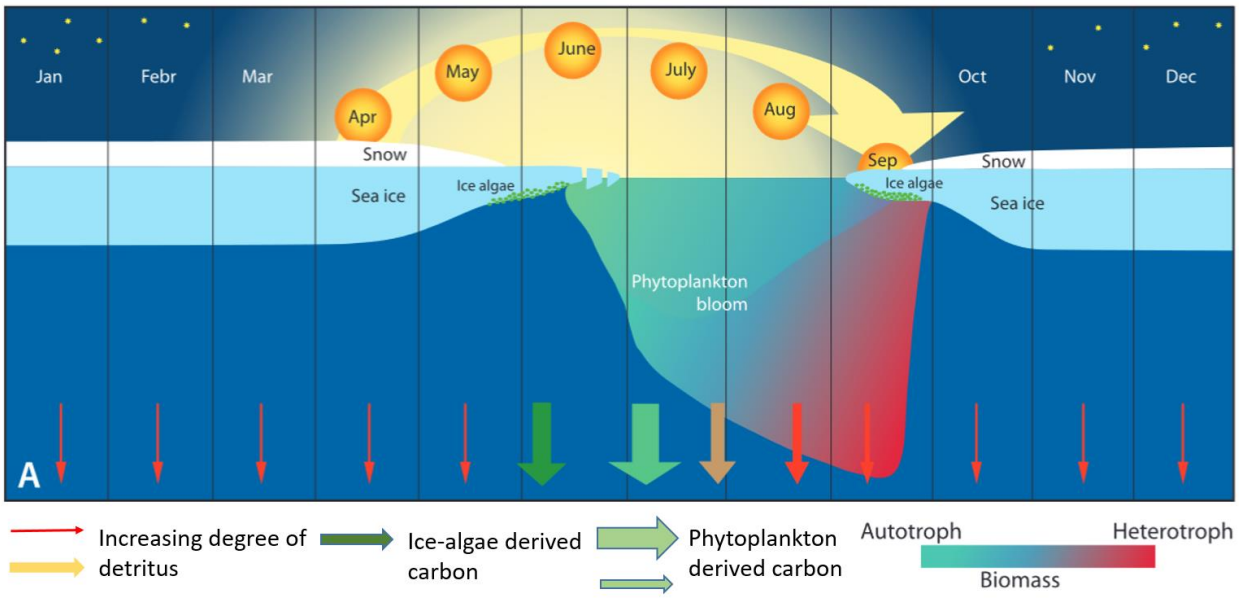

Figure 2. The seasonality in the bloom development and vertical flux of carbon in the Arctic Ocean is shown. The thickness of the arrows shows the magnitude of the vertical flux (Modified from Wassmann & Reigstad, 2011).

There exists strong seasonality in higher altitudes, for example in the Barents Sea (79°N). The polar night starts in November and ends in February at 79°N (Figure 2, Wassmann & Reigstad, 2011) during which the sun remains 12° below horizon (Berge et al., 2015) . The sea-ice cover is maximum in March-April after that it declines (Leu et al., 2011). Seasonality in the region is mainly governed by sea ice-cover which controls the seasonality by limiting the light, hence influencing the primary production by sea-ice algae (Wassmann et al., 2006). Under seasonal ice covered waters, the ice along with the snow-cover reduce the productive season than ice-free waters (Wassmann et al., 2006). The first algal bloom can be observed in high altitudes like 79°N during Late-April-June, followed by the phytoplankton bloom during July-August (Leu et al., 2011; Wassmann & Reigstad, 2011). Thinning of the ice sheet or earlier melting increases the light penetration to the water and subsequently increases the primary production which can increase the vertical flux of carbon (Wassmann & Reigstad, 2011). After the sea-ice has melted, the dominancy in the water column shifts from autotrophs (sea-ice algae to phytoplankton) to heterotrophs (zooplanktons) (Wassmann & Reigstad, 2011a). The seasons in the high altitudes are difficult to determine and are subjected to change with global warming and climate change. However, based

upon the water column (upper) temperature in, the winter starts when the water temperature reaches to -1.8°C usually in February followed by thick sea-ice cover. The spring starts with the bloom in sea-ice algae (Late-April-June), followed by the summer (sea-ice free water). The autumn starts when the water gets warmed usually in September-December (Berge et al., 2015; Leu et al., 2011).

Environmental factors, such as temperature, light availability, and nutrient concentrations, profoundly influence the biological productivity of the region (Wassmann & Reigstad, 2011a). Their seasonal variations play an essential role in influencing the vertical flux of particulate sinking matter, encompassing both organic and inorganic materials. Understanding these fluctuations is important to comprehend the functioning of the ecosystem and the mechanisms governing the carbon pump.

1.3 The oceanic carbon pump

The Barents Sea is a thriving ecosystem, with diverse species, ranging from microscopic phytoplankton to iconic species such as the Beluga Whale (*Delphinapterus leucas*). The regulation of atmospheric and aquatic carbon dioxide (CO_2) involves the Oceanic carbon pump. This process consists of the physical carbon pump which is responsible for the solubility of CO_2 from the atmosphere (Volk & Hoffert, 1985). The biological carbon pump (BCP) is further categorized into the organic carbon pump and carbonate pump (Volk & Hoffert, 1985). The organic carbon pump involves the vertical flux of the primary production, produced by ice and pelagic algae. The ice algae and phytoplankton are grazed by zooplankton and fish mostly in the euphotic zone. A fraction of the organic material undergoes re-mineralization here, while others move to the aphotic zone, where they are subsequently subjected to grazing and microbial degradation processes. This process leads to their dissolution and incorporation into the water column through re-mineralization, or they settle to the seabed. The settled organic matter is a food source for benthos and a portion of it is sequestered as shown in Figure 3 (Iversen, 2023; Wassmann et al., 2008).

Whereas, the carbonate pump involves the transformation of dissolved inorganic carbon (DIC) to calcium carbonate ($CaCO_3$) (Iversen, 2023). Marine planktonic calcifiers play an important role as they fix CO_3^{-2} and act as bio-indicators for ocean acidification (Anglada-Ortiz et al., 2021, 2023). Planktonic foraminifers incorporate CO_3^{-2} into their shells as calcite ($CaCO_3$), upon death, their bodies sink to the ocean floor and accumulate in the sediment as particulate inorganic carbon (PIC) Limacina helicina. After that, they are either sequestered or dissolved hence controlling the

carbon budget, and contributing in the carbon cycle (Schiebel, 2002). Whereas, the shells of planktonic pteropods are made up of aragonite which is a metastable form of $CaCO_3$, hence, are more sensitive towards ocean acidification than foraminifers (Bednaršek, Možina, et al., 2012). Their contribution in the vertical flux is higher but usually get dissolved due to the ocean acidification and hence contribute less carbon sequestration than foraminifers (Anglada-Ortiz et al., 2021).

Vertical flux refers to the vertical transport of particulate matter (particulate organic and inorganic matter), from the surface ocean to deeper layers, including the seafloor(Volk & Hoffert, 1985). This flux plays a significant role in the functioning of marine ecosystems and the cycling of essential elements (Lima et al., 2014; Volk & Hoffert, 1985). However, carbon sequestration occurs in the ocean floor, and subsequent resuspension reintroduces this stored carbon back into the system (Dybwad et al., 2022; Iversen, 2023). The composition of the vertical flux, as reflected in sinking particulate matter, chlorophyll a, planktonic marine calcifiers, and particulate organic carbon and nitrogen, aids in understanding the oceanic carbon pump and the impacts of environmental factors.

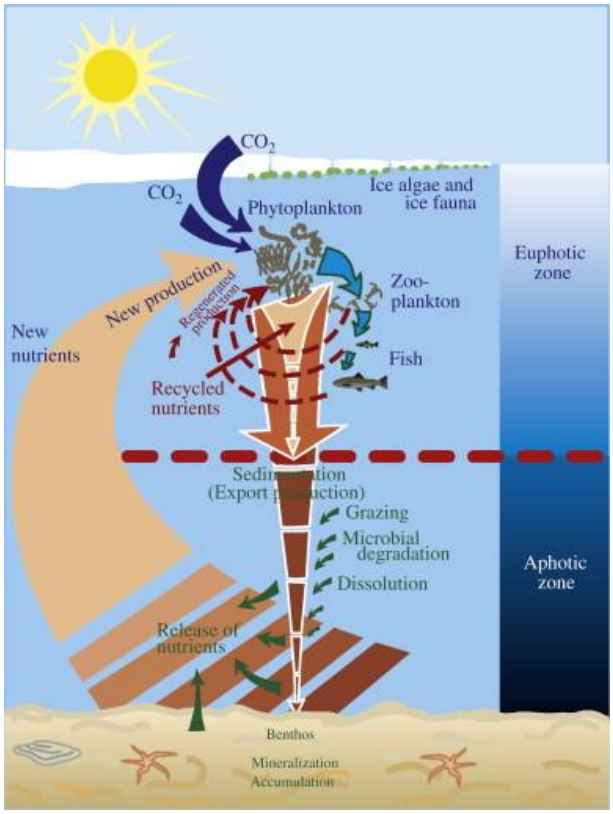

Figure 3. The summary of the biological carbon pump is shown in the figure (Wassmann et al., 2008).

1.4 Previous research and research gap

Long-term bottom moored sediment traps were mounted in the eastern Fram Strait for five years (2000-2005) to study the sedimentation pattern in this area. It was indicated that the vertical fluxes of particulate matter are seasonal, and carbonate shelled- animals contribute significantly to TPM especially carbonate flux (PIM). Also, the seasonality of the vertical fluxes is governed by the sea-ice and ambient hydrographical environments. The sea ice influence the primary production by impacting the light penetration and ambient hydrographical environments governs nutrient supply through stratification and vertical mixing (Bauerfeind et al., 2009).

The impacts of sea ice and the Atlantic Water on vertical flux were studied east and north of Svalbard by using sequential sediment traps. It was found that ice-free regions showed higher TPM

and particulate organic carbon (POC) fluxes than ice covered regions. Other factors like sunlight and grazers influenced vertical flux of organic matter. The primary production gets accelerated by sunlight hence increasing the algal biomass (increases chl a flux) whereas grazers feed upon the algal biomass which increases the degraded materials (increases organic matter flux) in the vertical flux of particulate matter (Dybwad et al., 2022).

The seasonal patterns of vertical flux were studied in the northwestern Barents Sea under AW inflow and sea ice by using short term sediment traps. The highest vertical fluxes were observed in May followed by August. They concluded that, even in the presence of smaller aggregates and reduced fresh material during the summer, the vertical flux can persist if fecal pellets sink efficiently and if mixing transports material to the seafloor (Bodur et al., 2023). Also, the seasonal distribution of the planktonic marine calcifiers (foraminifers and pteropods) and their contribution in vertical flux of carbon at seven stations (76°N to 82°N) in the northern Barents Sea were studied. It was found that calcifiers (especially *Limacina helicina*) contribute mainly in summer and autumn season and their contribution in carbon is higher at seasonally ice-covered stations than open water stations. This led to assumption about the potential increase in the export production in the region, particularly in October (Anglada-Ortiz et al., 2023). Furthermore, it was observed at north Svalbard stations that planktonic foraminfers and pteropods contribute three times more in PIM ($CaCO_3$) than POM (Anglada-Ortiz et al., 2021).

In addition, the seasonal patterns of the environmental factors like ocean currents, water inflow, temperature, salinity, sea ice conditions were observed at two stations in the northern Barents Sea (Lundesgaard et al., 2022), but the information on the full annual cycle of the vertical flux of particulate matter and composition was missing in this continental shelf region.

To address this issue, long-term sediment traps as part of the Nansen Legacy project, has been deployed at the Nansen Legacy M1 station, and these data will facilitate the investigation on the annual vertical flux and seasonal variability in this region.

1.5 Research questions

In the northern Barents Sea, the vertical flux is assumed to be influenced by the environmental conditions and biological processes, and this study focuses to answer these questions:

1) How do seasonal environmental patterns influence the vertical flux of total particulate matter and its organic and inorganic components in the Northern Barents Sea?

2) To what extent do planktonic marine calcifiers contribute to the vertical carbon flux, and how is their contribution influenced by seasonal variations, particularly during the summer season?

2 Study region

This study was conducted in the East of Svalbard and in the Northern Barents at M1 station (79°34.975N; 28°04.38E), downstream of Kvitøya Trough (Figure 3). McLane sediment trap model Mark 78H-21, with rotating bottles (Sundfjord & Renner, 2021), was deployed at one of the entrances of the Atlantic Ocean where the warm AW flows towards the Northern Barents Sea (Figure 4) (Lundesgaard et al., 2022). Physical parameters of this site were recorded by Lundsgaard et al. (2022). The oceanographic conditions are affected by the mixing of AW and PW and also by the surface water (due to sea-ice formation/melting) (Loeng, 1991; Lundesgaard et al., 2022). Other environmental factors such as wind and temperature also contribute in the maintenance of the oceanic conditions (Lundesgaard et al., 2022). The M1 area was partially ice covered from autumn 2019 to February 2020 (Figure 5 c, g), with an average sea ice concentration (SIC) fluctuating at approximately 50% (Figure 5c). Subsequently, from February 2020 to June 2020, it experienced full ice coverage, with an average SIC fluctuating at around 90%.

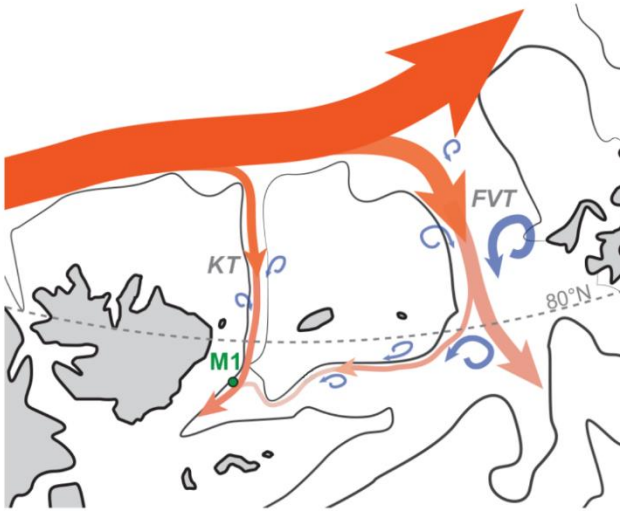

Figure 4. M1 represents the research station, orange arrow show the warm Atlantic water which subsequently cools down and blue arrows indicate the cold polar water (Modified from Lundesgaard et al., 2022)

The figure 6a, explain the sea-ice conditions at M1 station. At the time of the deployment (18 November), weak sea-ice cover was present. The sea-ice became dominant after February with few weak ice-covers and an open window during late-April and early-May and finally completely melts in July. The currents were directed mostly southwest until May, after that oppositely directed (Northeast), however, were directed southwest in July (Figure 6b). The surface temperature remained low during all months until July, in which it was warm (Figure 6d). Before February, the warm water dominated in the water column after that during the strong sea ice-cover, the cold water dominated (Figure 6c). The summer temperature varied in the water column (Figure 6d).

Subsequently, at start, the salinity in the upper (21m) water column was lower (<34gkg^{-1}) than the lower (<250m) water column (35gkg^{-1}) (Figure 6f) (Lundesgaard et al., 2022).

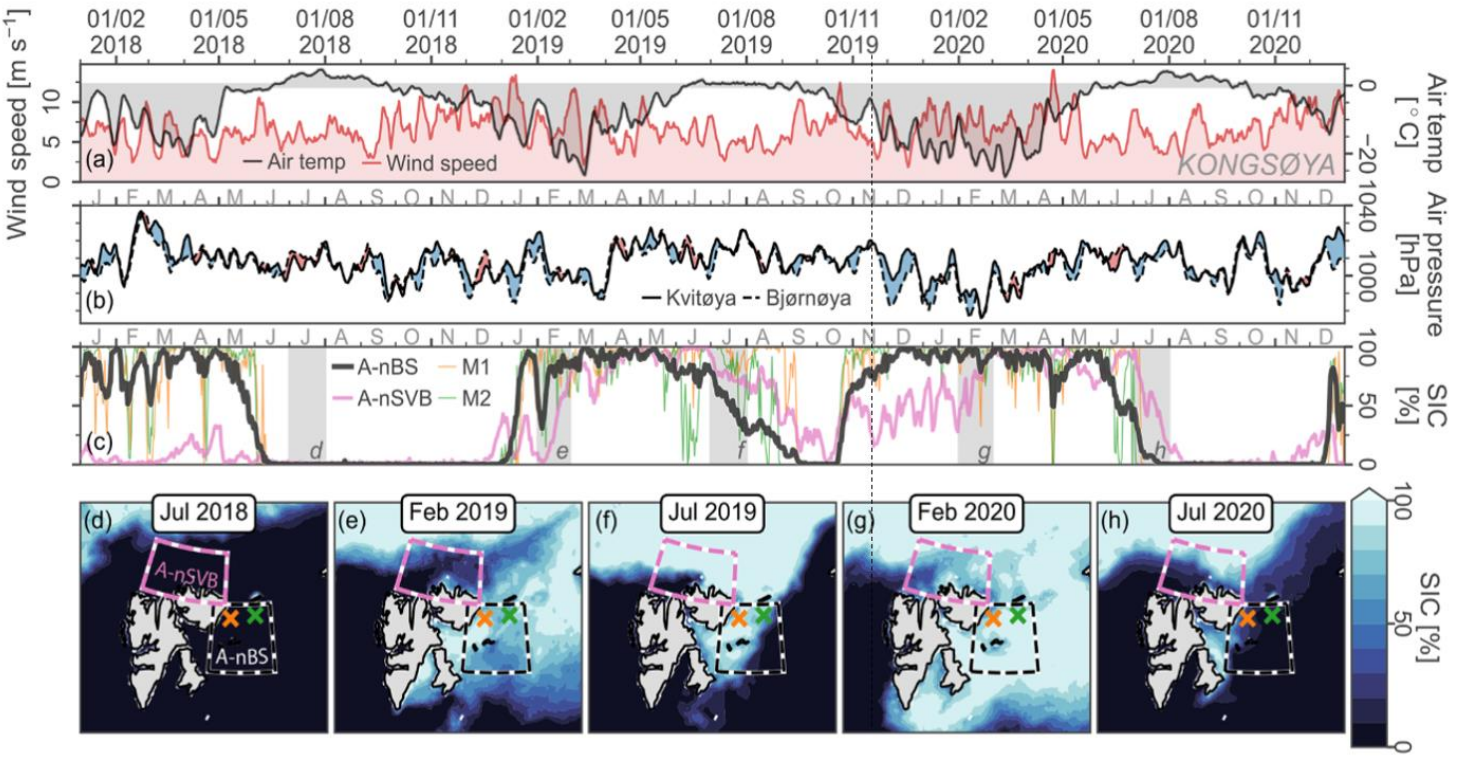

Figure 5. The atmospheric and sea ice conditions during 2018–2020 were examined through various data sources at M1 research station. a) Air temperature, b) Air pressure, c) Sea ice concentrations, and d-h) sea-ice conditions. Dotted line indicates the start (18 November) of the sediment trap and orange cross represents M1 station (Modified from Lundesgaard et al., 2022)

The salinity in this area started to decrease from 34.7gkg^{-1} during the melt season (April-onwards) and reached <31.9gkg^{-1} until August and then again started to increase (Figure 6 e, f) (Lundesgaard et al., 2022).

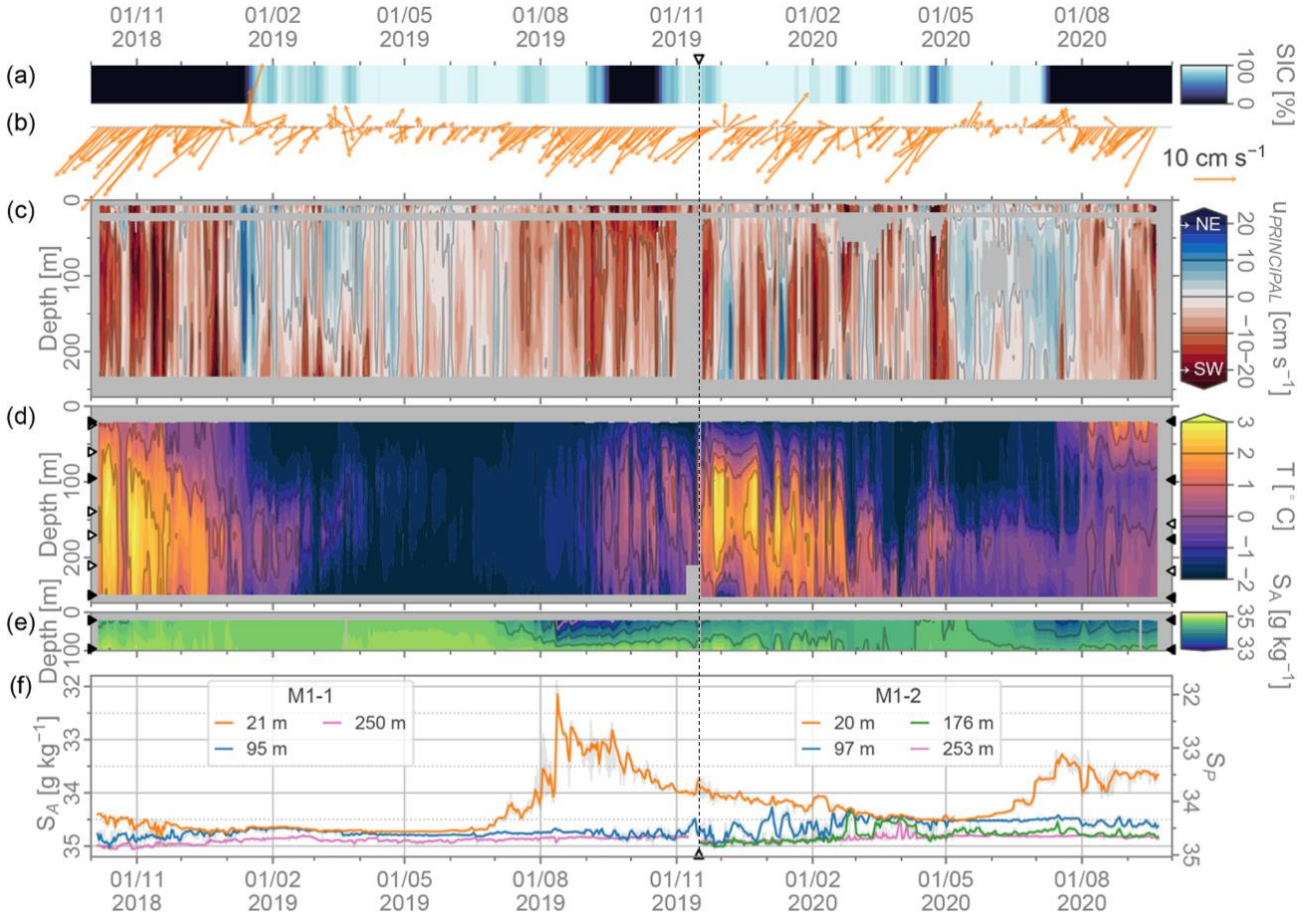

Figure 6. Weekly mean time series have been shown, recorded at M1. a) Sea ice concentrations (SIC), b) depth averaged current vector, c) current along the direction of maximum subtidal variance, d) in situ temperatures, e) absolute salinity in the upper 100m, f) absolute salinity recorded by individual sensors, the black dotted line indicates the start (18 November) of sediment trap (Modified from Lundesgaard et al., (2022).

The surface water was fresher in the absence of sea ice (due to the melting of sea ice) and saline under the ice cover due to the rejection of brine (Loeng, 1991; Lundesgaard et al., 2022).

3 Materials and Methods

3.1 Sample preparation and collection

The moored sediment traps were deployed at the Nansen Legacy M1 station in order to provide the vertical flux. The mooring was deployed 95m deep while the bottom depth was kept 265m.The moored trap contained 21 bottle (500ml each) containing prefixed sea water (Dybwad et al., 2022). Sea water (11L) for the sample was taken from ~196m depth with salinity of 34.85gkg^{-1}, was filtered using GF/F filters to avoid any particulate matter(Dybwad et al., 2022). Salinity of the

sample mixture was elevated by adding 5g of NaCl/liter. The total volume of 1100ml of hexamine buffered formaldehyde (37%) was added to 11L of filtered sea water with a final concentration of 4% formaldehyde. However, it was later discovered that hexamine has been used by mistake instead of borax as a buffer and resulted with implications for the particulate organic carbon and nitrogen (POC/PON) measurements. The bottles automatically changed after a pre-set interval; for each bottle the start date, end date and the number of days for which the bottle was opened are shown in Table 1(Sundfjord & Renner, 2021). The bottles were kept open for a shorter period of time during May and June to capture the spring bloom.

Table 1. Sampling periods for the 21 bottles sediment trap 2019-2020

Bottle No.	**Start date**	**End date**	**No. of Days**
1	18/11/2019	16/12/2019	28
2	16/12/2019	13/01/2020	28
3	13/01/2020	10/02/2020	28
4	10/02/2020	09/03/2020	28
5	09/03/2020	23/03/2020	14
6	23/03/2020	06/04/2020	14
7	06/04/2020	20/04/2020	14
8	20/04/2020	04/05/2020	14
9	04/05/2020	11/05/2020	7
10	11/05/2020	18/05/2020	7
11	18/05/2020	25/05/2020	7
12	25/05/2020	01/06/2020	7
13	01/06/2020	15/06/2020	14
14	15/06/2020	29/06/2020	14
15	29/06/2020	13/07/2020	14
16	13/07/2020	27/07/2020	14
17	27/07/2020	10/08/2020	14
18	10/08/2020	24/08/2020	14
19	24/08/2020	07/09/2020	14
20	07/09/2020	28/09/2020	21

21	28/09/2020	19/10/2020	21

3.2 Sub-sampling

After recovery each of the 21 bottles, each containing 500ml, was carefully homogenized and then split into two sets of 21 bottles, each containing 250ml, named as sub-samples A and B (Figure 7).

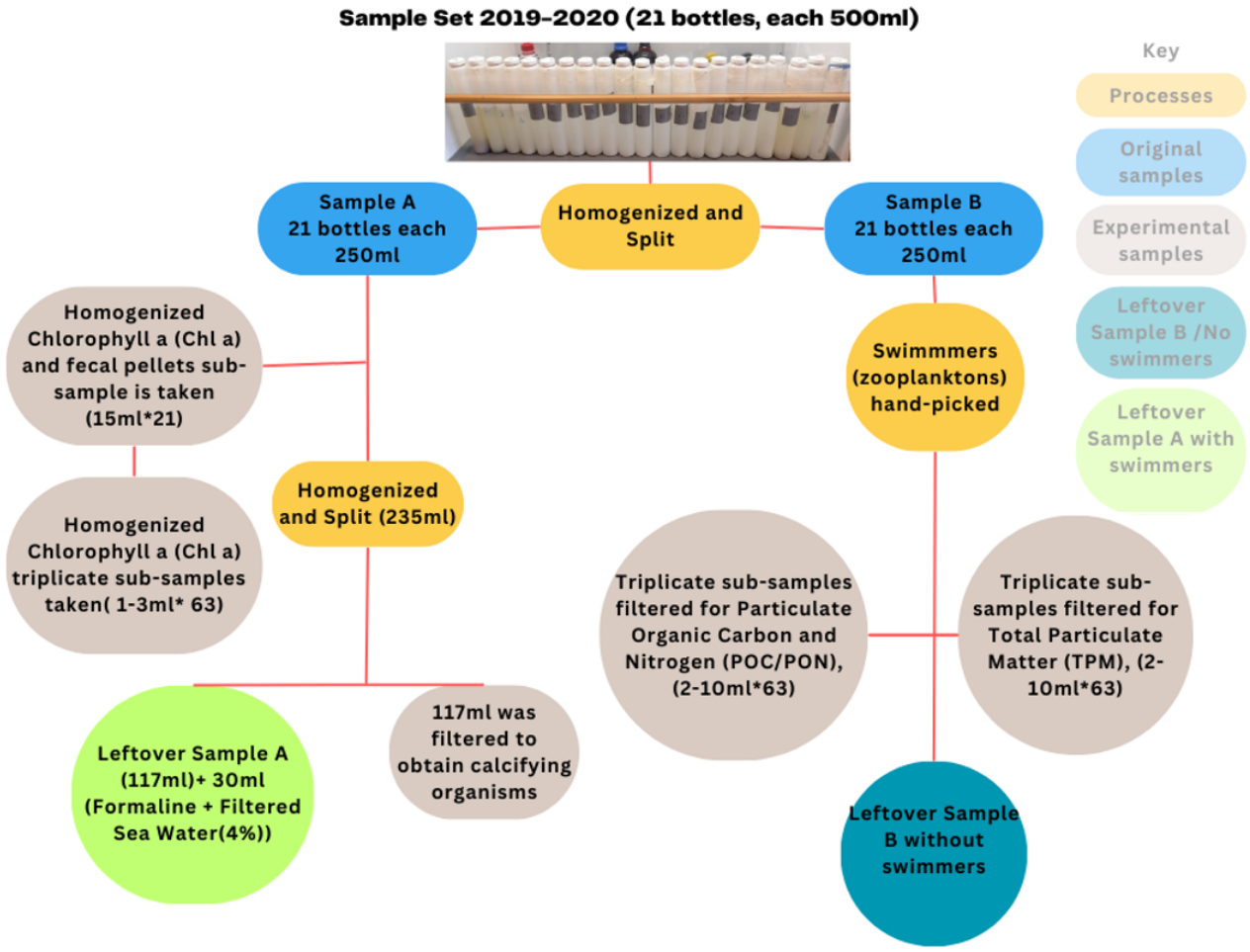

Figure 7. The process of sample splitting and the processes have been shown.

Both sample sets were kept in separate boxes and stored in dark at room temperature with proper ventilation to avoid any degradation caused by light. The original sample was split into two set and different sub samples were taken from these two previously split samples. Sub-samples for chlorophyll a (chl a) measurement (1-3ml) were taken from the sub-sample A as shown in the figure 5. A list of variables measured in this study is given in table 2 along with their category.

Table 2. List of variables included in the study

Total particulate matter and composition	
Particulate Organic Matter(POM)	Particulate Inorganic Matter(PIM)
Chlorophyll-a (Chl a) and phaeo-pigments Particulate Organic Carbon (POC) and Particulate Organic Nitrogen (PON)	The flux of Planktonic Marine Calcifiers as $CaCO_3$

The swimmers were manually removed from sample B (Table 3) and carefully picked with forceps to ensure that their presence did not impact the analysis of total particulate matter (TPM) and particulate organic carbon and nitrogen (POC/PON) (Wiedmann et al., 2020). The people along with their roles have been enlisted in Table 3.

Table 3. Shows the contributions of the research technicians from research group

Name	Contribution
Miriam Marquardt	Split the sample set, hand-picked the swimmers(zooplankton) by using forceps
Ulrike Dietrich	Calibrated the fluorimeter on 21.01.22 Operated the CHN analyzer and analyzed a preliminary set of samples for particulate organic carbon and nitrogen (POC/PON)
Tassawer Hussain	Sample preparation for POC/PON, chlorophyll a, TPM, and planktonic marine calcifiers, stable isotopes, Highly branched isoprenoids (HBIs), Fecal pallets. Analysis of TPM and chl a, microscopy for calcifiers and analysis, data entry, data analysis with R and thesis writing

3.3 Total Particulate Matter and Composition

The materials used were, Whatman GF/F blank filters (0.7µm, diameter 25mm) being packed in aluminum sheets, aluminum sheets sliced into small pieces and aluminum cups. Filters, aluminum sheets and aluminum cups were combusted for 7hrs at 450°C to remove any organic material

(Wassmann, 1991). The blank filters were weighed after combustion and packed in combusted and sliced aluminum pieces with a tracking number and stored in airtight container for future use. The weight was noted under the blank weight (W_{blank}). Aluminum cups were also assigned a tracking number and stored. Triplicates sub samples were filtered on pre-weighed and combusted filters, subsequently rinsed by Milli-Q water to remove any salt present in the sample, and finally spread on combusted aluminum cups and then dried for ~24hrs at 60^{o}C (Wassmann, 1991). Then, the filters were taken out and re-weighed by using microbalance and noted under the weight before combustion (W_{bc}). Total particular matter (TPM) was quantified after subtracting the blank filter weight (W_{blank}) from the raw weight of filter (W_{bc}) by using equation 1 (Dybwad et al., 2022). Then the filters were burned at 450^{o}C for 7hrs to combust any organic matter present on the filter (Wassmann, 1991). The filters were weighed again and noted under the weight after combustion (W_{ac}) and W_{ac} was subtracted from the TPM to measure particulate inorganic matter (PIM) by using the equation 2. Particulate organic matter (POM) is the difference between TPM and PIM as shown in equation 4 (Dybwad et al., 2022). The raw values were divided by the sample volume (L) to obtain the concentration in mg/L The filters were acclimated before weighing and made sure that all samples were treated in the same way. All of the measurements were recorded in mg/L.

$$TPM(mg/L) = \frac{W_{bc} - W_{blank}}{Filtered\ Volumn(L)} \quad (1)$$

$$PIM(mg/L) = \frac{TPM - W_{ac}}{Filtered\ Volumn(L)} \quad (2)$$

$$POM(mg/L) = TPM - PIM \quad (3)$$

3.4 Chlorophyll a

Quantification of chl a is the direct measurement of healthy algal cells while phaeo-pigments are the degradation or by-product of the algal cells, either after being eaten or simple degradation. Chl a to phaeo-pigments ratio depicts the health of the algal cells. High chl a/phaeo-pigments means most of the algae is healthy and little degraded and vice versa. The conical plastic tubes were filled with 5ml 100% methanol each and assigned a tracking number subsequently placed in refrigerator. Then, the triplicate subsamples for chl a and phaeo-pigments were filtered on non-combusted GF/F filters (Bodur et al., 2023; Lalande et al., 2014), picked by forceps while folded inward (to avoid any contamination and loss of materials) and put in the relevant plastic tubes. The samples were

placed at ~4°C to extract the pigments for 12-24hrs (Dybwad et al., 2022). Chl a is sensitive towards light and may undergo degradation process. Keeping the samples in cold and dark during extraction helps to prevent the degradation of the pigments. Then, the samples were taken out, acclimated at room temperature in dark for around 30min and the analysis started. Before starting the analysis, Trilogy Fluorimeter was calibrated against a commercially available calibration standard (Sigma, C6144) (Dybwad et al., 2022). At first, the samples were put on a vortex mixer for few seconds to detach the pigments from the filter, immediately transferred the contents into a new test tube. Then, the raw concentrations of chl a were measured by using pre-calibrated fluorimeter (Turner Trilogy Fluorimeter) (Butler, 1984).

Secondly, the sample was removed from the fluorimeter and two drops of 5% hydrochloric acid (HCl) were added to denature any phycobiliproteins present in the sample and let the sample sit for 60-90s (Butler, 1984). Phycobiliproteins interfere with the chl a measurement by absorbing the similar wavelengths to chl a.The denaturation process is completed usually in 1-1.5min. At the end, after homogenization, the raw values of chl a as relative fluorescence units (RFU) were measured. For the precision and accuracy of the data, after every 10 samples, blank samples (containing 100% methanol) are measured to correct for any noise or background fluorescence in the fluorimeter (Dybwad et al., 2022). Fluorescence detection (FD) refers to the process of detecting fluorescence emission from a sample. Fluorescence Lifetime (Tau τ), denotes the mean duration a fluorophore remains in the excited state before releasing a photon and returning to the ground state. RFU is a relative measure of the fluorescence intensity emitted by a sample, used for comparisons between different samples or conditions (Huot & Babin, 2010). Chl a and phaeo-pigments values were noted and compiled in .xlsx format. During calculation blank values were subtracted from the raw data and the concentrations (mg m) for chl a and phaeo-pigments were calculated by using equation 4 and 5 (Butler, 1984).

$$Chl\ a\ (concentration) RFU = \frac{Fd \times tau \times (Rb - Ra) \times Methanol(ml)}{sub\ sample(ml)} \quad (4)$$

$$Phaeopigments\ (concentration)\ RFU = \frac{Fd \times tau \times \left(\left(\frac{Rb}{Ra} \times Ra\right) - Rb\right) \times Methanol(ml)}{sub\ sample(ml)} \quad (5)$$

Where, Fd= 0.000399, tau = 1.917, Rb= RFU before HCl, Ra= RFU after HCl, Rb/Ra = 2.095. Fd, tau and Rb/Ra are constant for a specific substance (Methanol).

3.5 Planktonic Marine Calcifiers

Sample A was once again split in to two using a motodo plankton sample splitter, capacity 1.5L. Half of the sample was sieved using a 64µm sieve. The filtrate was rinsed by filtered sea water to avoid organisms from bursting due to the tonicity and transferred to a plastic container. The calcifiers were counted using LEICA (LAS X MZ165) with camera and inverted light source (LED). The planktonic foraminifers and pteropods were picked manually, using a fine brush and deposited in black background slides. The pteropods were further classified as *Limacina helicina* and *Limacina retroversa*. Photographs were taken at different magnifications for example, 1.25x-6x for pteropods and 8x-11x for foraminifers due to their smaller sizes, a reference bar was drawn in each photograph and were analyzed by using imageJ software (Schneider, et at. 2012). The biomass of *Limacina helicina* (*L. helicina*), *Limacina retroversa (L. retroversa)* and foraminifers were quantified by equation 6, 7 (Bednaršek et al., 2012b), and 8 by using the shell length (Bednaršek et al., 2012a; Meilland et al., 2018) respectively and multiplied by number of organisms found in each. Then the biomass was transformed to carbon by multiplying it with a conversion factor of 0.25 (Larson, 1986). For *Limacina retroversa* only, the wet weight by multiplied by 0.28 to obtain dry weight (Bednaršek et al., 2012; Davis & Wiebe, 1985). Inorganic carbon was obtained by subtracting organic carbon from the total carbon and was done by multiplying with 0.27 and 0.73 for *Limacina helicina* and *Limacina* retroversa, respectively (Bednaršek et al., 2012b). Inorganic carbon was quantified as calcium carbonate ($CaCO_3$) by multiplying inorganic carbon to 8.33 which is the molecular mass ratio as shown in equation 9 (Bednaršek et al., 2012a). The data was documented in .xlsx format and processed in R.

$$Limacina\ helicina\ biomass\ = (0.137 \times D^{1.5005}) \quad (6)$$

$$Limacina\ retroversa\ biomass = (0.000194 \times D^{2.5473}) \quad (7)$$

$$Foraminfera\ biomass = (2.04 \times 10^{-5} x^{2.2}) \quad (8)$$

$$\text{Calcium cabonate} = (\text{Total carbon} - \text{Total organic carbon}) \times 8.33 \quad (9)$$

Where D is the diameter (l) of the organisms, x is the shortest length compared to diameter in foraminifera, and 8.33 is the molecular mass ratio of carbon in $CaCO_3$.

3.6 Particulate Organic Carbon and Nitrogen

Particulate organic carbon and nitrogen (POC/PON) triplicate subsamples were filtered on combusted GF/F filters (Whatman, 0.7 μm with 25mm diameter), taken from sub-sample B (without swimmers). The blank filters were combusted for 7hrs at 450°C to remove any organic carbon present on to the GF/F filters to avoid any misperception in the results (Dybwad et al., 2022; Wassmann, 1991). After observing the concentrations of the sample based upon the coloration on the filter, the sub-sampling volume ranged from 2-10ml (2ml for the most dark samples and 10ml for the light samples) (Wassmann, 1991). The triplicates were packed in small pieces of combusted aluminum foil and stored in a plastic bag containing a tracking number. The triplicate filters were then frozen at -80°C soon after being packed until further process (Dybwad et al., 2022). For the analysis of POC/PON, the filters were taken out, put in labeled glass tubes, arranged in a test tube holding rack, and were dried at 60°C for 24hrs (Dybwad et al., 2022). All the steps and procedures were recorded. Dried triplicates were exposed to acid fumes to eliminate any inorganic carbon (C) for 24hrs and then again dried at 60°C. Then, triplicate filters were packed in Nickel capsules and were stored in a desiccator until they were analyzed by using a CHN elemental analyzer (Exeter Analytical CE440) (Dybwad et al., 2022).

3.7 Flux Calculation

The vertical flux was calculated separately for each parameter using the following calculations.

3.7.2 Total Particulate Matter flux calculation:

TPM, PIM and POM concentrations were converted into vertical flux of carbon as shown in the equations (10, 11, and 12)

$$TPM\ flux(mgm^{-2}d^{-1}) = \frac{TPM(concentration) \times Trap\ volume\ (L)}{Trap\ area(m^2) \times No.of\ Days} \qquad (10)$$

$$PIM\ flux(mgm^{-2}d^{-1}) = \frac{PIM(concentration) \times Trapvolume\ (L)}{Trap\ area\ (m^2) \times No.of\ Days} \qquad (11)$$

$$POM\ flux(mgm^{-2}d^{-1}) = \frac{POM(concentration) \times Trap\ volume\ (L)}{Trap\ area\ (m^2) \times No.of\ Days} \qquad (12)$$

3.7.1 Chlorophyll a flux calculation:

Chlorophyll a (equation 13) and phaeo-pigment (equation 14) concentrations were quantified into vertical flux of carbon in terms of chl a and phaeopigments as:

$$Chl\ a\ \ flux\ (mgm^{-2}d^{-1}) = \frac{Chl\ a(concentration) \times Trap\ volume(L)}{1000 \times Trap\ area\ (m^2) \times No.of\ Days(Day)} \qquad (13)$$

$$Phaeopigments\ flux\ (mgm^{-2}d^{-1}) = \frac{phaeo(concentration) \times Trap\ volume(L)}{1000 \times Trap\ area(m^2)\ \times No.of\ Days(Day)} \qquad (14)$$

Where, trap volume: 0.5L, Trap area: 0.5m^2, no. of days: days the bottle was kept open (Table 1)

3.7.3 $CaCO_3$ flux calculation:

Contribution of the planktonic marine calcifying organisms in the vertical flux of inorganic carbon as $CaCO_3$ was calculated as shown in equation 15:

$$CaCO3\ flux\ (mgm^{-2}d^{-1})\ = \frac{Concentrations \times Trap\ volume}{Trap\ area \times filtered\ volume \times No.of\ Days} \qquad (15)$$

3.7.4 The Annual Vertical flux

The annual vertical flux was calculated by multiplying the vertical flux of each sample with the days (the bottle was opened). Last bottle closed on 19/10/2020 so, November was missing. It was assumed that the values were same for October and November due to almost same environmental conditions. So, the vertical flux in October is also used for November to make a complete year (365 days).

3.7.5 Particulate Organic Carbon and Nitrogen (POC/PON):

The resulted raw values of POC/PON were abnormal which was later discovered that it was the result of hexamine buffered solution. The resulted carbon to nitrogen ratios were less than 2.5 (1.5-2.36) due to the high values of carbon and nitrogen. While the ratios were expected to be >6 according to Redfield ratio (Tett et al., 1985). The reason, hexamine is itself so rich in carbon and nitrogen which affected the results, so, the raw values of POC/PON were not usable. Therefore, no further processes were done with these values.

3.7.6 Computer programs/data analysis tools

The data was compiled in Microsoft excel 2016 while data cleaning and processing was done by R 3.3.0+ and R studio 2022.12.0+353. The output was generated as plots and tables.

4. Results

4.1 Total Particulate Matter and Composition:

The highest vertical flux of total particulate matter (mg TPM m^{-2} d^{-1}) was observed in December, (45.32mg TPM m^{-2} d^{-1}) during early winter season and then second highest flux in June (41.22 mg TPM m^{-2} d^{-1}) during late spring season and third peak can be observed during autumn in September (25.76 mg TPM m^{-2} d^{-1}) as shown in figure 8a. Standard deviations are the error bars of triplicate sub samples (n=3) shown in figure 8a. The pattern of annual vertical flux of TPM shows that it is maximum in December (45.32mg TPM m^{-2} d^{-1}), then starts to decline until March (17.02 mg TPM m^{-2} d^{-1}) and then shows some increment and start inclining and reach up to the maximum flux in June (41.22 mg TPM m^{-2} d^{-1}).

Then, TPM fluxes decline until becomes minimum in August (3.2 mg TPM m^{-2} d^{-1}) and shows the last peak in September (25.76 mg TPM m^{-2} d^{-1}). Particulate inorganic matter (PIM) contributes more than particulate organic matter (POM) in the vertical flux of TPM, throughout the year and especially in the winter from December-April (Figure 8b). The overall vertical flux of both POM and PIM start declining after December and show

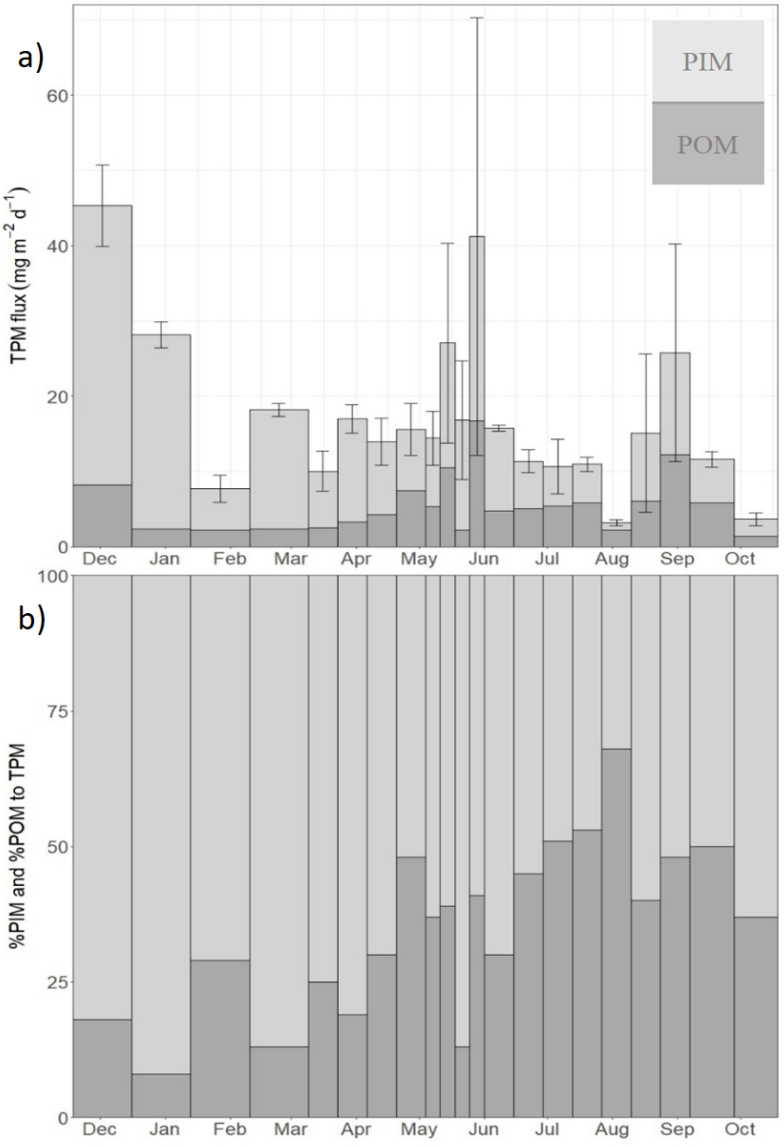

Figure 8. The vertical flux of TPM given as mg TPM m^{-2} $d^{-1}$and the composition (PIM and POM) from 18-11-2019 to19-10-2020, with error bars where n=3, are shown in the figure. b) The relative contribution of POM and PIM to TPM are shown in percentages.

variations in the flux until again incline in the spring and in summer but declines in late summer (Figure 8a). The lowest value for PIM is in August (1.02 mg PIM m^{-2} d^{-1}) and highest in December (37.11 mg PIM m^{-2} d^{-1}) while that for POM is in October (1.37 mg POM m^{-2} d^{-1}) and June (16.72 mg POM m^{-2} d^{-1}) respectively. PIM deposition is more in winter and less in summer. Whereas, POM shows a gradual incline as compared to PIM but varies when the value of the flux is taken into account.

This trend has been further illustrated in figure 8b where %POM and %PIM to total TPM have been shown. During December %POM and % PIM are 18% and 82%, respectively. This is followed by the lowest and highest percentages of POM and PIM in January, 8% and 92% respectively. Although the %PIM is > 50% in all the months except in August, %POM has shown an incline starting from January (18%) to maximum in August (68%). The PIM shows overall higher percentages in winter (the highest of 82% in January) than summer (32% in August) while POM shows overall higher percentages during summer (the highest of 68% in August) than in winter (8% in January).

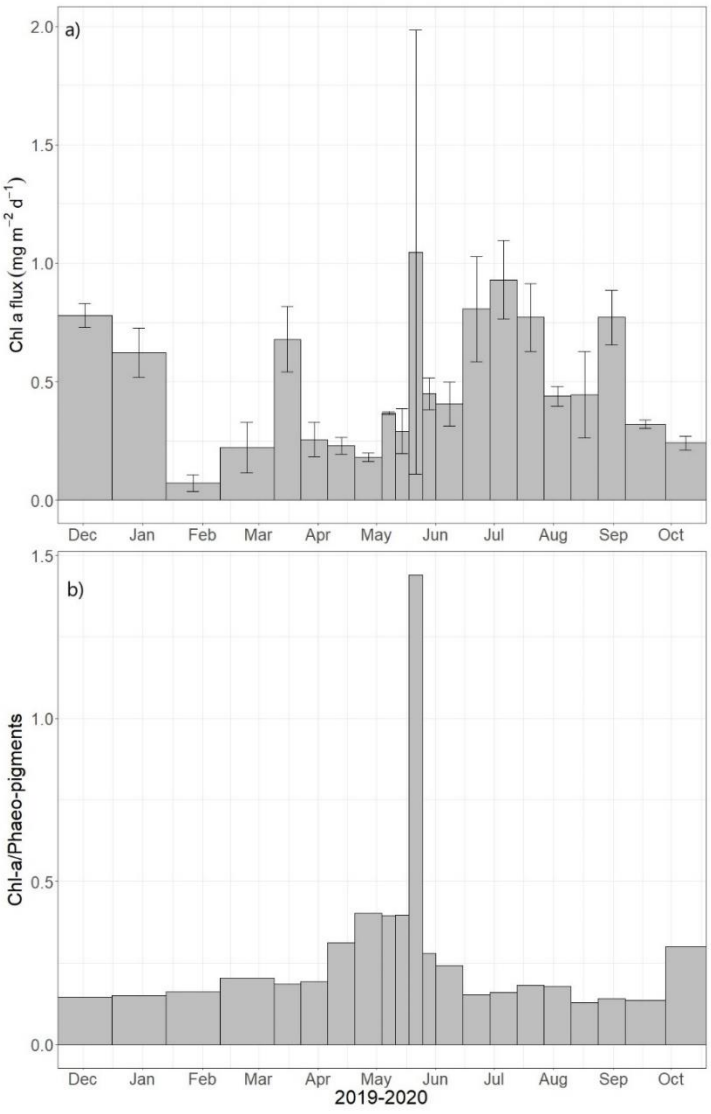

Figure 9. a) The seasonal pattern of vertical flux of Chl a, during the period November 2019-October 2020 is shown with error bars where n=3. b) The seasonal pattern of Chl a/phaeo-pigments ratio is shown.

4.2 Chlorophyll a and phaeo-pigments vertical flux:

Seasonal pattern of vertical flux of Chl a is shown in figure 9a. Standard deviations are the error bars of triplicate sub samples (n=3) shown in Figure 9a. During winter December-February, there is a rapid decline from 0.77 mg m^{-2} d^{-1} in December to 0.07 mg m^{-2} d^{-1} in February (also the lowest)

and then it starts to incline and reaches to the highest vertical flux of Chl a, observed as 1.04 mg m^{-2} d^{-1} in early June.

It decreases to 0.40 mg m^{-2} d^{-1} in late June and then again increases in July (0.77 mg m^{-2} d^{-1}) and then starts to decline and reaches to 0.43 mg m^{-2} d^{-1} in August. Followed by an inclines (0.77 mg m^{-2} d^{-1}) in September and then declines to 0.24 mg m^{-2} d^{-1} in October. Chl a follows almost the same pattern (figure 9a) as POM (Figure 8a). Figure 4b demonstrates the Chl a/phaeo-pigments ratio. The ratio is < 0.16 until February after that, it increases in March and reaches to 0.20. From April to onwards, it starts to increase and the highest value of 1.44 has been observed in June. Then, the ratio becomes almost constant <0.20, until it reaches to 0.30 in late October (autumn).

4.3 Planktonic Marine Calcifiers

Certain samples were selected to understand the contribution of planktonic marine foraminifers and pteropods (*Limacina helicina* and *Limacina retroversa*) in the vertical flux of carbon as $CaCO_3$. The overall deposition of calcifiers is low during the winter and higher in the summer as can be seen in figure 10. *L. helicina* has been deposited throughout the year and in selected sample, with highest deposition flux of 252.9 ind m^{-2} day^{-1} in September and the lowest of 3 ind m^{-2} day^{-1} in August.

It has almost same flux of individuals, found in December (17.3 ind m^{-2} day^{-1}) and January (17.9 ind m^{-2} day^{-1}) followed by a decrease in late January (5.47 ind m^{-2} day^{-1}). It shows an incline from March (9.11 ind m^{-2} day^{-1}) to May (6 ind m^{-2} day^{-1}) then declines to the lowest flux in Augut followed by the highest flux in September. The deposition flux of *Limacina retroversa* is more in winter showing the highest flux of 61.4 ind m^{-2} day^{-1} in February followed by January (13.7 ind m^{-2} day^{-1}) than in spring (1.21 ind m^{-2} day^{-1} in June). However, no deposition flux has been recorded after June. The last value in October in figure 10 corresponds to zero value. Foraminifers show highest deposition flux in December (50.8 ind m^{-2} day^{-1}) followed by July (14 ind m^{-2} day^{-1}), April (10.3 ind m^{-2} day^{-1}) and September (3 ind m^{-2} day^{-1}) respectively (figure 10).

Shell size or the length of the PMC show a seasonal trend as can be seen in figure 11a. The average length for *Limacina retroversa* is the highest in February (1.05 mm) followed by March (1.03 mm) and the lowest in December (0.74 mm). *Limacina helicina* shows an incline starting form 0.58 mm in December, followed by 0.68 mm in January and continue increasing until 1.77 mm in July (the highest). Then it declines to 0.52 mm in August followed by the lowest of 0.45 mm in September

(Figure 11a). Foraminifers possess a value of 0.14 mm in December, 0.15 mm in February, and the highest value of 0.23mm in April, and maintains the shell size between 0.21-0.13 mm from June to October (Figure 11a).

Figure 10. The figure shows the vertical flux as ind $m^{-2}day^{-1}$ for the corresponding sample throughout the year for pteropods (Limacina helicina and Limacina retroversa) and foraminifers. * means no data

The contribution of planktonic marine calcifiers (foraminifers and pteropods) in the vertical flux of inorganic carbon flux as $CaCO_3$ has been shown in figure 11b. The vertical flux of $CaCO_3$ is <1.06 mg m^{-2} d^{-1} in winter than spring (up to 7.19 mg m^{-2} d^{-1}) and summer (up to 7.13 mg m^{-2} d^{-1}). The highest flux of $CaCO_3$ has been observed during autumn in September (8.08 mg m^{-2} d^{-1}) and the lowest vertical flux is in August (0.12 mg m^{-2} d^{-1})

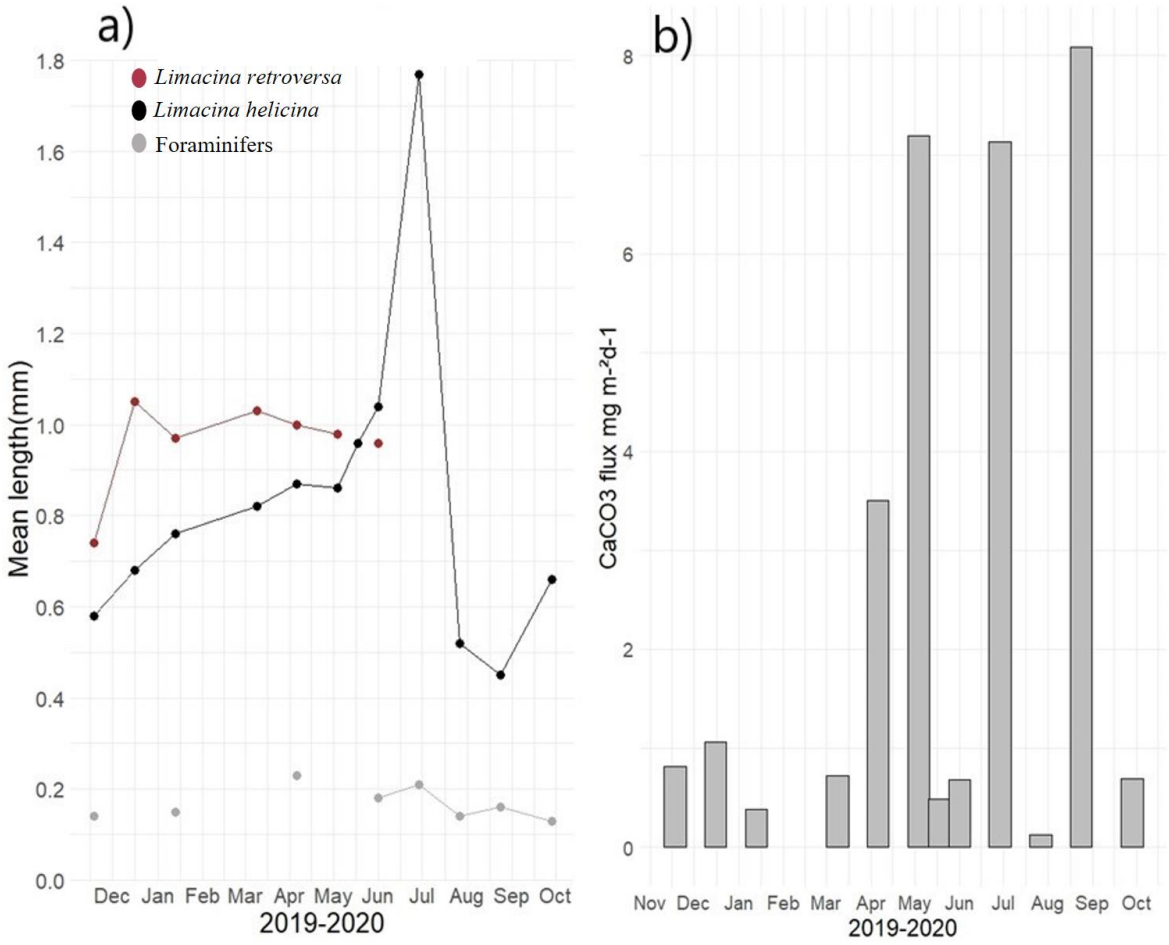

Figure 11. a) the trend of shell sixe or the length of the organisms b) the seasonal pattern of vertical flux of planktonic marine calcifiers as $CaCO_3$

The percentage of $CaCO_3$ to PIM has been shown in figure 12. The percentage of $CaCO_3$ to PIM is increasing from December (2.2%) to May (79 %) , then it drops to 3.3% in early June and again starts increasing and reach to 100% in July then again decreases to 11.7% and shows an increase again in September (59%) and finally drops to 30.2% in October.

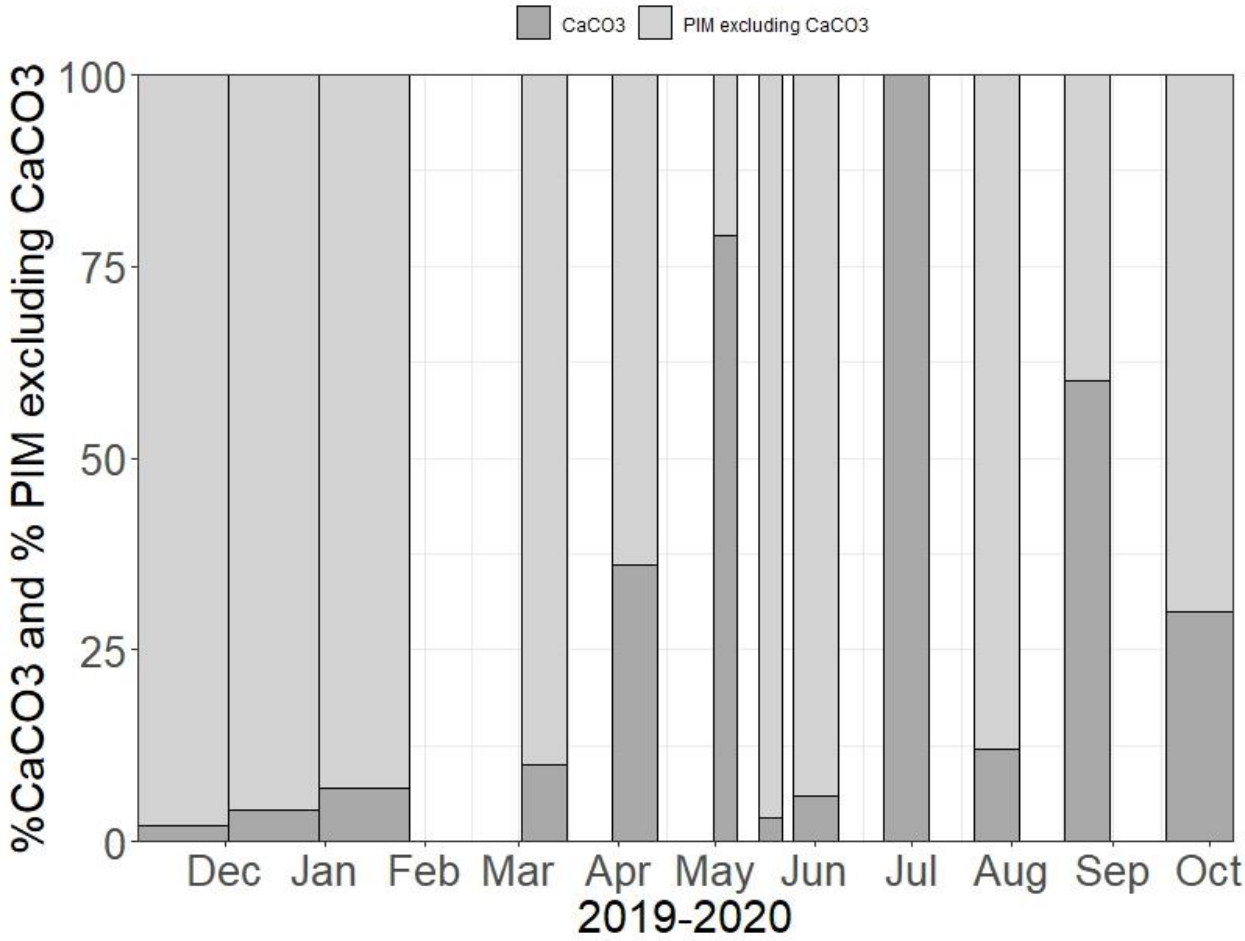

Figure 12. Relative contribution of calcifiers as CaCO3 to PIM given as % has been shown.

4.4 The Annual Vertical flux

The annual vertical flux of TPM has been found ~5.96 g m^{-2} $year^{-1}$. The PIM contribute ~ 4.29 g m^{-2} $year^{-1}$ and POM contribute ~1.67 g m^{-2} $year^{-1}$ to the TPM. The annual vertical flux of chl a has been found ~ 0.16 g m^{-2} $year^{-1}$ and calcifiers contribute ~ 0.42 g m^{-2} $year^{-1}$

5. Discussion

The study exhibits a strong seasonal influence of the environmental factors on the vertical flux of various particulate matter components and the contribution of planktonic marine calcifiers to the vertical carbon flux, shedding light on the complex dynamics within the northern Barents Sea. Total Particulate Matter (TPM) demonstrated distinct peaks in winter (December) and late spring (June) while showing a steady decline in summer (August) with an additional peak in autumn (September). Particulate Inorganic Matter (PIM) displayed higher fluxes during winter, the highest

in December, contrasting with Particulate Organic Matter (POM) that exhibited a more gradual increase, reaching its maximum during summer (June) and autumn (September). These variations between PIM and POM fluxes emphasize their differential contributions and responses to seasonal changes. Particularly, the seasonal pattern of POM showed a resemblance to Chlorophyll a (Chl a) flux, underlining a potential connection between organic matter and phytoplankton biomass. Calcifiers were less dominant during winter and contributed in the vertical flux of PIM mainly during the summer and autumn season with highest flux in September.

5.1 The Vertical Flux during winter

The highest vertical flux of TPM is in December when, the station is under weak sea ice and dark (figure 2 and 6). Major portion of TPM comes from PIM which might be advected by the Atlantic Water (AW) inflow because the direction of the currents was southwest (toward the station) during that period as shown in figure 6b (Lundesgaard et al., 2022). Also, the calcifiers, especially foraminifera flux is the highest in December which contributed in PIM flux and could be another possible reason for this such high PIM contribution to TPM (Figure 10 and 11b). Also, the POM contributes significantly to the vertical flux of TPM in December which is mostly advected by the AW inflow (supported by the currents) (Lundesgaard et al., 2022) and resuspension during early winter (Dybwad et al., 2022). The contribution of the phytoplankton biomass is minute as compared to the other organic matter because chlorophyll a flux is 0.77 mg m^{-2} d^{-1} in December which is <10% of the total POM in December. Most of the phytoplankton biomass was degraded and aged as suggested by the low chl a/phaepigments ratio (figure 9 a,b).

In January, the station is under sea ice and the TPM flux declines but the %PIM is the highest, meaning that the %POM is the lowest (8 a,b). The strong currents are responsible for vertical flux in two ways, 1) by advecting TPM along with AW (Lundesgaard et al., 2022) , and 2) by causing resuspension (Dybwad et al., 2022; Lalande et al., 2014). Because of negligible primary production, chl a flux is also low and the low value of chl a/phaeo-pigments suggests that POM was both suspended and advected (Figure 9 a, b). The PIM is also assumed to be advected by the AW water, locally contributed by other species and re-suspended. Planktonic marine calcifiers are also assumed to be advected by the AW inflow. However, the contribution of foraminifers and pteropods to PIM as $CaCO_3$ is low. Contrarily, almost 3.6 and 5.5 times less TPM flux has been observed in the north (~12.5 mg m^{-2} d^{-1}) before Kvitøya Trough and east (< 8 mg m^{-2} d^{-1}) just after

Kvitøya Trough respectively, in Svalbard (81°N) during December-January (2017-2018) (Dybwad et al., 2022).

5.2 The Vertical Flux under sea ice and in spring

From February-May, the current direction and strength is same but the TPM flux shows declined variations until May. The sea-ice cover has been established, meanwhile the polar night ends, and the sun shines in early March (Figure 2). The PIM portion of TPM has shown comparatively lower flux then previous months, and the POM flux has started to show a slight incline (Figure 8 a, b). However, in the north and east of Svalbard (2017-2018), highest vertical flux of TPM has been observed during mid-February-March (~137.5 mg m^{-2} d^{-1}) and February-mid March (~51 mg m^{-2} d^{-1}), respectively (Dybwad et al., 2022). It was after a high mixing event during winter so PIM has been the main contribution in the vertical flux of TPM (Dybwad et al., 2022).

The sea-ice algae grows under low light intensity beneath the ice and also being dependent on the solar angle hence, is mainly considered sole contributor to the primary production during this period (figure 2) (Leu et al., 2011). The polar day (late-April to Late July) (Berge et al., 2015) accelerates the primary production by sea-ice algae. From February to May, the current direction and strength remain consistent, yet the Total Particulate Matter (TPM) flux exhibits a declining trend until May. During this period, sea-ice cover is established, polar night ends, and the onset of sunlight in early March (Figure 2). Although the Particulate Inorganic Matter (PIM) portion of TPM shows a comparatively lower flux, there is a slight increase in the flux of Particulate Organic Matter (POM). Sea-ice algae, is assumed the primary contributor to the primary production in this period, thrives under low light intensity beneath the ice and is influenced by the solar angle (Leu et al., 2011; Wassmann & Reigstad, 2011).

The polar day, spanning from late April to late July (Berge et al., 2015), accelerates primary production by sea-ice algae and pelagic algae. Variations in chlorophyll a (chl a) flux beneath the sea ice signify the algal bloom, typically occurring from March to June in higher latitudes (79°N) (Leu et al., 2011; Wassmann & Reigstad, 2011). This period also witnesses the emergence of ice-free or weakened ice cover areas, such as melt ponds (Figure 6a) (Lundesgaard et al., 2022; Polashenski et al., 2012; Wassmann & Reigstad, 2011b), contributing to observed variations, notably a slight increase in POM flux (Figure 9a,b). The contributions of ice-algae and pelagic algae to chl a flux vary, but beneath sea ice, ice-algae is assumed to be dominant. These variations

are particularly influenced by the flux of chlorophyll a, with the increase in the chl a/phaeo-pigments ratio further reinforcing these observations (Figure 9 a, b).

The contribution of calcifiers to PIM as $CaCO_3$ is low during February-March and contribute significantly during April-May with higher in May as compared to the previous months (figure 11b and 12). In the north and east of Svalbard the chl a flux is highly low during this period (2017-2018 (Dybwad et al., 2022). The sea-ice cover is still present and the currents are directed northeast which means the low AW influence at the station (Lundesgaard et al., 2022). So, most of the TPM flux is supposed to be local.

In June, spring bloom contributes to the second highest vertical flux of TPM with higher POM contribution than previous months. In the north and east of Svalbard, the chl a flux is higher during June and a decline in the nitrate concentrations is documented which reveals it as spring bloom (Dybwad et al., 2022). The marginal ice zone in higher latitudes experience spring bloom (by ice algae) under sea ice usually just before the ice-melt and is usually proceeded two months prior to the pelagic bloom (figure 2) (Leu et al., 2011). However, the spring and pelagic algal blooms can vary depending upon the sea ice melting (Leu et al., 2011). The vertical flux of chl a is the highest in June which is caused by the peak of spring algal bloom, supported by the highest ratio of chl a/phaeo-pigments. However, very less PIM is contributed by calcifiers, documented by the low $CaCO_3$ flux.

5.4 The vertical flux during the summer

The study area becomes ice free in July, the cold and less saline polar water dominates and the surface salinity declines (figure 6 a, c, e). From late June to early August (2020), the vertical flux of TPM and the composition is almost constant. The flux of chl a is between 1 and 0.75 mg m^{-2} day^{-1} and low chl a/phaeo-pigments ratio suggests that these are mostly degraded pigments (figure 2,8 and 9). The chl a/phaeo-pigments ratios are almost same for rest of the period with few variations in August and show peak in October (figure 9 a,b). The low values chl a/phaeo-pigments are either by grazing or degradation (or both) in the water-column due to sluggish sinking. The grazers are more active during summer season and their life cycles depend upon the algal blooms (Leu et al., 2011). In July, calcifiers contribute to PIM more than 100% which might be due to the over-estimation of calcifiers, possibly caused by the sample splitting. In August, the AW inflow returns and the AW dominates in the water column. The polar day ends and the system is assumed

to be exhausted and deprived of nutrients required for primary production resulting the lowest TPM flux in August. In the north Svalbard (2017-2018) a decline in the chl a flux and continuous decline in the nitrate concentration support this exhaustion (Dybwad et al., 2022). However in the east of Svalbard (2017-2018), the highest chl a flux has been observed in August (Dybwad et al., 2022). It can be concluded that the nutrient concentrations vary with altitude and time of the year. In the current study, both PIM and POM are low in August and the contribution of %POM is the highest in August and %PIM contribution is the lowest in August, although the southwestern currents return (Figure 8 a, b).

5.5 The Vertical Flux in autumn

The last seasonal variations in the vertical flux of TPM are seen in autumn (September-December). The area is ice free with strong southwest currents, mainly driving the variation in TPM (Lundesgaard et al., 2022) (figure 5 and 6) and the nitrate concentrations start to increase (2017-2018) (Dybwad et al., 2022). However, the TPM flux is lower in the north of Svalbard in September (2017-2018) as compared to this study (2019-2020) (Dybwad et al., 2022) The POM decrease has been associated with the lack of nutrients in late August (Dybwad et al., 2022) but TPM shows the last peak in September caused by high chl a (POM) flux (figure 9 a,b) and $CaCO_3$ (PIM) contributed by the calcifiers (figure 11b and 12). In September, the chl a flux is high but with low chl a/phaeo-pigments ratio suggesting the modification of algal biomass by the grazers (Figure 2) (Wassmann & Reigstad, 2011). The chl a flux in October is lower than September but the chl a/phaeo-pigments ratios are higher in October than September suggesting the absence or less activity of the grazers (Bodur et al., 2023). It is revealed that the carbon export by the calcifiers declines in October but increased export was hypothesized about the north of Svalbard (Anglada-Ortiz et al., 2023)

5.6 The annual vertical flux of Particulate matter and composition

In this study, the annual vertical flux of TPM is ~5.96 g m^{-2} $year^{-1}$ which is 2.16 times lower than the annual sedimentation (12.92 g m^{-2}) in summer (2004-2005) and almost five times lower than the annual sedimentation (32.09 g m^{-2}) in summer (2002-2003) at in Fram Strait (Bauerfeind et al., 2009). The annual TPM fluxes at north and east of Svalbard (2017-2018) are 9.14 g m^{-2} $year^{-1}$ and 4.20 g m^{-2} $year^{-1}$ respectively (Dybwad et al., 2022) so the annual flux in the current study (~5.96 g m^{-2} $year^{-1}$) is lower than the north Svalbard station but higher than the east Svalbard station. The annual PIM flux in the current study is ~ 4.29 g m^{-2} $year^{-1}$ which contribute 71.97% with 9.79%

contribution from the annual $CaCO_3$ flux (~ 0.42 g m^{-2} $year^{-1}$) to the TPM. The annual $CaCO_3$ flux contribute 7.04% to the annual TPM flux. At Fram Strait, during summer 2002-2003 and 2004-2005, the $CaCO_3$ flux contributed 18% and 17% to the total matter flux respectively (Bauerfeind et al., 2009) which is higher than that found in the current study. The difference can be due to the geographical location of both stations and the years because the ocean dynamics (currents and other environmental conditions) vary from year to year.

The annual PIM fluxes found at north and east of Svalbard (2017-2018) are 7.21 g m^{-2} $year^{-1}$ and 3.09 g m^{-2} $year^{-1}$ respectively (Dybwad et al., 2022). The flux at north of Svalbard is higher but the flux at east is lower than that found the current study (~ 4.29 g m^{-2} $year^{-1}$). The possible reasons can be, 1) due to the influence of the AW, 2) due to re-suspension, 3) the pattern of the oceanic currents which may vary from year to year and season to season and 4) a small branch is diverted to the southwest from Kvitøya Trough just before the east Svalbard station (Dybwad et al., 2022), weakening the main current. The foraminifers size range and pattern is almost same as found (2021) east to the station (current) and pteropods shell sizes are > 0.6mm but those found east of Svalbard are mostly < 0.6mm except in December (when > 0.6mm) (Anglada-Ortiz et al., 2021).

The annual chl a flux in this study has been found ~ 0.162 g m^{-2} $year^{-1}$ and the annual chl a fluxes found at north and east of Svalbard (2017-2018) are 0.21 g m^{-2} $year^{-1}$ and 0.165 g m^{-2} $year^{-1}$ (Dybwad et al., 2022). The northern station has higher chl a flux because it was ice-free during the study period (2017-2018) than seasonally ice-covered eastern station with lower chl a flux (Dybwad et al., 2022). The chl a flux found in this study is almost same to the eastern Svalbard station (2017-2018) only with a minute difference of 0.003 g m^{-2} $year^{-1}$. This is because both of the stations were seasonally ice-covered and possibly less availability and early depletion of the nitrates as documented in the previous study (2017-2018) (Dybwad et al., 2022).

5.7 Vertical Flux regulation

The vertical flux of total particulate is regulated by several biotic and abiotic factors and processes. The seasonality of the sea-ice and the availability of the nutrients influence (by increasing/decreasing) the vertical flux of particulate matter (PIM and POM) (Lalande et al., 2014). In addition, the advection of the water masses, tidal mixing and resuspension increases the vertical flux of total particulate matter (Dybwad et al., 2022; Lalande et al., 2014). The zooplanktons (grazers) contribute and regulate the vertical flux of POM by grazing on the algal

biomass and by producing fecal pallets. The overgrazing by zooplanktons will decrease the chl a flux in the vertical flux but fecal pallets will increase the POM (Bodur et al., 2023). The absence of grazers or the mis-match between the onset of primary production and the life cycles of the grazers significantly influence the vertical flux of POC by increasing chl a flux and decreasing fecal pallet flux (Bodur et al., 2023). The primary production is reduced in the absence of nitrates but becomes negligible in the absence of light (Bednaršek, et al., 2012b; Leu et al., 2011). The sea-ice algae is reliant on on the existence of sea ice and zooplanktons species have linked their life cycles with the onset of sea-ice algae bloom rather than pelagic bloom (Leu et al., 2011).

6 Conclusions

In conclusion, this study unravels the intricate seasonal dynamics influencing the vertical flux of particulate matter and the significant contribution of planktonic marine calcifiers in the northern Barents Sea. Total Particulate Matter (TPM) displayed distinct peaks during winter and late spring, gradually declining in summer, and exhibiting a final peak in autumn. The interplay between Particulate Inorganic Matter (PIM) and Particulate Organic Matter (POM) showcased varied responses to seasonal changes. Furthermore, chlorophyll a flux aligned with POM, emphasizing a potential link between organic matter and phytoplankton biomass. Planktonic foraminifers and pteropods contributed, notably during summer and autumn, highlighting their seasonal significance. The outcomes of this study shed light on the complex interactions of environmental factors, including sea-ice dynamics, nutrient availability, and zooplankton grazing, in regulating the vertical flux of particulate matter. Moreover, the annual analysis revealed the overall contribution of the system to the carbon flux, with PIM, POM, chl a, and calcifiers playing distinctive roles. The comparison with other regions underscores the regional variability in flux patterns, influenced by local ocean dynamics.

References

Anglada-Ortiz, G., Meilland, J., Ziveri, P., Chierici, M., Fransson, A., Jones, E., & Rasmussen, T. L. (2023). Seasonality of marine calcifiers in the northern Barents Sea: Spatiotemporal distribution of planktonic foraminifers and shelled pteropods and their contribution to carbon dynamics. *Progress in Oceanography, 218*, 103121. https://doi.org/10.1016/j.pocean.2023.103121

Anglada-Ortiz, G., Zamelczyk, K., Meilland, J., Ziveri, P., Chierici, M., Fransson, A., & Rasmussen, T. L. (2021). Planktic Foraminiferal and Pteropod Contributions to Carbon Dynamics in the Arctic Ocean (North Svalbard Margin). *Frontiers in Marine Science, 8*. https://www.frontiersin.org/articles/10.3389/fmars.2021.661158

Bauerfeind, E., Nöthig, E.-M., Beszczynska, A., Fahl, K., Kaleschke, L., Kreker, K., Klages, M., Soltwedel, T., Lorenzen, C., & Wegner, J. (2009). Particle sedimentation patterns in the eastern Fram Strait during 2000–2005: Results from the Arctic long-term observatory HAUSGARTEN. *Deep Sea Research Part I: Oceanographic Research Papers*, *56*(9), 1471–1487. https://doi.org/10.1016/j.dsr.2009.04.011

Bednaršek, N., Možina, J., Vogt, M., O'Brien, C., & Tarling, G. A. (2012). The global distribution of pteropods and their contribution to carbonate and carbon biomass in the modern ocean. *Earth System Science Data*, *4*(1), 167–186. https://doi.org/10.5194/essd-4-167-2012

Bednaršek, N., Tarling, G. A., Fielding, S., & Bakker, D. C. E. (2012). Population dynamics and biogeochemical significance of Limacina helicina antarctica in the Scotia Sea (Southern Ocean). *Deep Sea Research Part II: Topical Studies in Oceanography*, *59–60*, 105–116. https://doi.org/10.1016/j.dsr2.2011.08.003

Berge, J., Renaud, P. E., Darnis, G., Cottier, F., Last, K., Gabrielsen, T. M., Johnsen, G., Seuthe, L., Weslawski, J. M., Leu, E., Moline, M., Nahrgang, J., Søreide, J. E., Varpe, Ø., Lønne, O. J., Daase, M., & Falk-Petersen, S. (2015). In the dark: A review of ecosystem processes during the Arctic polar night. *Progress in Oceanography*, *139*, 258–271. https://doi.org/10.1016/j.pocean.2015.08.005

Bodur, Y. V., Renaud, P. E., Goraguer, L., Amargant-Arumí, M., Assmy, P., Maria Dąbrowska, A., Marquardt, M., Renner, A. H. H., Tatarek, A., & Reigstad, M. (2023). Seasonal patterns of vertical flux in the northwestern Barents Sea under Atlantic Water influence and sea-ice decline. *Progress in Oceanography*, *219*, 103132. https://doi.org/10.1016/j.pocean.2023.103132

Butler, E. I. (1984). A manual of chemical and biological methods for sea water analysis. *Deep Sea Research Part A. Oceanographic Research Papers*, *31*(12), 1523. https://doi.org/10.1016/0198-0149(84)90086-4

Carmack, E., Barber, D., Christensen, J., Macdonald, R., Rudels, B., & Sakshaug, E. (2006). Climate variability and physical forcing of the food webs and the carbon budget on panarctic shelves. *Progress in Oceanography*, *71*(2), 145–181. https://doi.org/10.1016/j.pocean.2006.10.005

Davis, C. S., & Wiebe, P. H. (1985). Macrozooplankton biomass in a warm-core Gulf Stream ring: Time series changes in size structure, taxonomic composition, and vertical distribution. *Journal of Geophysical Research: Oceans*, *90*(C5), 8871–8884. https://doi.org/10.1029/JC090iC05p08871

Drinkwater, K. F. (2011). The influence of climate variability and change on the ecosystems of the Barents Sea and adjacent waters: Review and synthesis of recent studies from the

NESSAS Project. *Progress in Oceanography*, *90*(1), 47–61. https://doi.org/10.1016/j.pocean.2011.02.006

Dybwad, C., Lalande, C., Bodur, Y. V., Henley, S. F., Cottier, F., Ershova, E. A., Hobbs, L., Last, K. S., Dąbrowska, A. M., & Reigstad, M. (2022). The Influence of Sea Ice Cover and Atlantic Water Advection on Annual Particle Export North of Svalbard. *Journal of Geophysical Research: Oceans*, *127*(10), e2022JC018897. https://doi.org/10.1029/2022JC018897

Huot, Y., & Babin, M. (2010). Overview of Fluorescence Protocols: Theory, Basic Concepts, and Practice. In D. J. Suggett, O. Prášil, & M. A. Borowitzka (Eds.), *Chlorophyll a Fluorescence in Aquatic Sciences: Methods and Applications* (pp. 31–74). Springer Netherlands. https://doi.org/10.1007/978-90-481-9268-7_3

Iversen, M. H. (2023). Carbon Export in the Ocean: A Biologist's Perspective. *Annual Review of Marine Science*, *15*(1), 357–381. https://doi.org/10.1146/annurev-marine-032122-035153

Lalande, C., Nöthig, E.-M., Somavilla, R., Bauerfeind, E., Shevchenko, V., & Okolodkov, Y. (2014). Variability in under-ice export fluxes of biogenic matter in the Arctic Ocean. *Global Biogeochemical Cycles*, *28*(5), 571–583. https://doi.org/10.1002/2013GB004735

Larson, R. J. (1986). Water content, organic content, and carbon and nitrogen composition of medusae from the northeast Pacific. *Journal of Experimental Marine Biology and Ecology*, *99*(2), 107–120. https://doi.org/10.1016/0022-0981(86)90231-5

Leu, E., Søreide, J. E., Hessen, D. O., Falk-Petersen, S., & Berge, J. (2011). Consequences of changing sea-ice cover for primary and secondary producers in the European Arctic shelf seas: Timing, quantity, and quality. *Progress in Oceanography*, *90*(1), 18–32. https://doi.org/10.1016/j.pocean.2011.02.004

Lima, I. D., Lam, P. J., & Doney, S. C. (2014). Dynamics of particulate organic carbon flux in a global ocean model. *Biogeosciences*, *11*(4), 1177–1198. https://doi.org/10.5194/bg-11-1177-2014

Loeng, H. (1991). Features of the physical oceanographic conditions of the Barents Sea. *Polar Research*, *10*(1), 5–18. https://doi.org/10.3402/polar.v10i1.6723

Loeng, H., & Drinkwater, K. (2007). An overview of the ecosystems of the Barents and Norwegian Seas and their response to climate variability. *Deep Sea Research Part II: Topical Studies in Oceanography*, *54*(23), 2478–2500. https://doi.org/10.1016/j.dsr2.2007.08.013

Lundesgaard, Ø., Sundfjord, A., Lind, S., Nilsen, F., & Renner, A. H. H. (2022). Import of Atlantic Water and sea ice controls the ocean environment in the northern Barents Sea. *Ocean Science*, *18*(5), 1389–1418. https://doi.org/10.5194/os-18-1389-2022

Meilland, J., Schiebel, R., Lo Monaco, C., Sanchez, S., & Howa, H. (2018). Abundances and test weights of living planktic foraminifers across the Southwest Indian Ocean: Implications for carbon fluxes. *Deep Sea Research Part I: Oceanographic Research Papers*, *131*, 27–40. https://doi.org/10.1016/j.dsr.2017.11.004

Polashenski, C., Perovich, D., & Courville, Z. (2012). The mechanisms of sea ice melt pond formation and evolution. *Journal of Geophysical Research: Oceans*, *117*(C1). https://doi.org/10.1029/2011JC007231

Reigstad, M., Wexels Riser, C., Wassmann, P., & Ratkova, T. (2008). Vertical export of particulate organic carbon: Attenuation, composition and loss rates in the northern Barents Sea. *Deep Sea Research Part II: Topical Studies in Oceanography*, *55*(20), 2308–2319. https://doi.org/10.1016/j.dsr2.2008.05.007

Schiebel, R. (2002). Planktic foraminiferal sedimentation and the marine calcite budget. *Global Biogeochemical Cycles*, *16*(4), 3-1-3–21. https://doi.org/10.1029/2001GB001459

Schneider, C. A., Rasband, W. S., & Eliceiri, K. W. (2012). NIH Image to ImageJ: 25 years of image analysis. *Nature Methods*, *9*(7), Article 7. https://doi.org/10.1038/nmeth.2089

Serreze, M. C., & Meier, W. N. (2019). The Arctic's sea ice cover: Trends, variability, predictability, and comparisons to the Antarctic. *Annals of the New York Academy of Sciences*, *1436*(1), 36–53. https://doi.org/10.1111/nyas.13856

Sundfjord, A., Assmann, K. M., Lundesgaard, Ø., Renner, A. H. H., Lind, S., & Ingvaldsen, R. B. (2020). Suggested water mass definitions for the central and northern Barents Sea, and the adjacent Nansen Basin: Workshop Report. *The Nansen Legacy Report Series*, *8*, Article 8. https://doi.org/10.7557/nlrs.5707

Sundfjord, A., & Renner, A. (2021). Mooring service cruise 2019. *The Nansen Legacy Report Series*, *19*. https://doi.org/10.7557/nlrs.5797

Tett, P., Droop, M. R., & Heaney, S. I. (1985). The Redfield Ratio and Phytoplankton Growth Rate. *Journal of the Marine Biological Association of the United Kingdom*, *65*(2), 487–504. https://doi.org/10.1017/S0025315400050566

Volk, T., & Hoffert, M. I. (1985). Ocean Carbon Pumps: Analysis of Relative Strengths and Efficiencies in Ocean-Driven Atmospheric CO2 Changes. In *The Carbon Cycle and Atmospheric CO2: Natural Variations Archean to Present* (pp. 99–110). American Geophysical Union (AGU). https://doi.org/10.1029/GM032p0099

Walsh, J. E., Overland, J. E., Groisman, P. Y., & Rudolf, B. (2011). Ongoing Climate Change in the Arctic. *AMBIO*, *40*(1), 6–16. https://doi.org/10.1007/s13280-011-0211-z

Wassmann, P. (1991). Sampling and Analysis of Marine Particles with Pebenoco (Pelagic-Benthic Coupling in the Norwegian Coastal Zone), University of Tromsø,Norway. In

Marine Particles: Analysis and Characterization (pp. 97–99). American Geophysical Union (AGU). https://doi.org/10.1029/GM063p0097

Wassmann, P., Carroll, J., & Bellerby, R. G. J. (2008). Carbon flux and ecosystem feedback in the northern Barents Sea in an era of climate change: An introduction. *Deep Sea Research Part II: Topical Studies in Oceanography*, *55*(20), 2143–2153. https://doi.org/10.1016/j.dsr2.2008.05.025

Wassmann, P., & Reigstad, M. (2011a). Future Arctic Ocean Seasonal Ice Zones and Implications for Pelagic-Benthic Coupling. *Oceanography*, *24*(3), 220–231.

Wassmann, P., & Reigstad, M. (2011b). Future Arctic Ocean Seasonal Ice Zones and Implications for Pelagic-Benthic Coupling. *Oceanography*, *24*(3), 220–231.

Wassmann, P., Reigstad, M., Haug, T., Rudels, B., Carroll, M. L., Hop, H., Gabrielsen, G. W., Falk-Petersen, S., Denisenko, S. G., Arashkevich, E., Slagstad, D., & Pavlova, O. (2006). Food webs and carbon flux in the Barents Sea. *Progress in Oceanography*, *71*(2), 232–287. https://doi.org/10.1016/j.pocean.2006.10.003

Wiedmann, I., Ershova, E., Bluhm, B. A., Nöthig, E.-M., Gradinger, R. R., Kosobokova, K., & Boetius, A. (2020). What Feeds the Benthos in the Arctic Basins? Assembling a Carbon Budget for the Deep Arctic Ocean. *Frontiers in Marine Science*, *7*. https://www.frontiersin.org/articles/10.3389/fmars.2020.00224

Appendix 1

Data for TPM Plots

The table represents the data for the TPM flux, bottle number = sample number corresponding to the start and closing date of the sample and no_days is the number of days the bottle was kept open. Tpm_mean represents the mean value of the triplicates and tpm_sd is the standard deviation. Followed by PIM mean and PIM standard deviation, POM mean and standard deviation and TPM, PIM and POM annual vertical fluxes.

bottle_nu	start_date	end_date	no_days	tpm_mea	tpm_sd	pim_mea	pim_sd	pom_mea	pom_sd	Tpm_annual	pim_annu	pom_annual
1	2019-11-18 00:00:00	2019-12-16 00:00:00	28	45.3214	5.38075	37.1143	2.82761	8.20714	2.5588083	1269	1039.2	229.8
2	2019-12-16 00:00:00	2020-01-13 00:00:00	28	28.1476	1.74028	25.7929	2.62107	2.35476	4.3014612	788.133333	722.2	65.9333
3	2020-01-13 00:00:00	2020-02-10 00:00:00	28	7.70357	1.81693	5.50119	1.57683	2.20238	0.2732162	215.7	154.033	61.6667
4	2020-02-10 00:00:00	2020-03-09 00:00:00	28	18.206	0.84353	15.8036	0.51973	2.40238	0.4356606	509.766667	442.5	67.2667
5	2020-03-09 00:00:00	2020-03-23 00:00:00	14	10.0548	2.68302	7.52619	2.43613	2.52857	0.248362	140.766667	105.367	35.4
6	2020-03-23 00:00:00	2020-04-06 00:00:00	14	17.0262	1.89266	13.7524	1.66637	3.27381	0.2268162	238.366667	192.533	45.8333
7	2020-04-06 00:00:00	2020-04-20 00:00:00	14	13.9333	3.1297	9.70238	2.56129	4.23095	0.6250034	195.066667	135.833	59.2333
8	2020-04-20 00:00:00	2020-05-04 00:00:00	14	15.5929	3.46172	8.15952	1.42974	7.43333	2.8852045	218.3	114.233	104.067
9	2020-05-04 00:00:00	2020-05-11 00:00:00	7	14.431	3.58046	9.10079	2.97766	5.33016	3.0536958	101.016667	63.7056	37.3111
10	2020-05-11 00:00:00	2020-05-18 00:00:00	7	27.0762	13.2439	16.5286	8.11148	10.5476	5.4078992	189.533333	115.7	73.8333
11	2020-05-18 00:00:00	2020-05-25 00:00:00	7	16.8	7.89041	14.5619	2.64461	2.2381	10.327626	117.6	101.933	15.6667
12	2020-05-25 00:00:00	2020-06-01 00:00:00	7	41.2238	29.0947	24.4952	16.5423	16.7286	12.685714	288.566667	171.467	117.1
13	2020-06-01 00:00:00	2020-06-15 00:00:00	14	15.7571	0.43513	11.0262	0.41159	4.73095	0.0250849	220.6	154.367	66.2333
14	2020-06-15 00:00:00	2020-06-29 00:00:00	14	11.3619	1.52473	6.27143	0.63354	5.09048	0.8928381	159.066667	87.8	71.2667
15	2020-06-29 00:00:00	2020-07-13 00:00:00	14	10.6476	3.60523	5.26667	2.42893	5.38095	1.1789249	149.066667	73.7333	75.3333
16	2020-07-13 00:00:00	2020-07-27 00:00:00	14	10.981	0.92704	5.13571	0.75461	5.84524	0.1787618	153.733333	71.9	81.8333
17	2020-07-27 00:00:00	2020-08-10 00:00:00	14	3.20952	0.43194	1.02897	0.61888	2.18056	0.618572	44.9333333	14.4056	30.5278
18	2020-08-10 00:00:00	2020-08-24 00:00:00	14	15.1286	10.4971	9.06905	8.54045	6.05952	2.125049	211.8	126.967	84.8333
19	2020-08-24 00:00:00	2020-09-07 00:00:00	14	25.7643	14.4422	13.5262	8.9921	12.2381	5.4529918	360.7	189.367	171.333
20	2020-09-07 00:00:00	2020-09-28 00:00:00	21	11.6222	1.05358	5.82698	0.08913	5.79524	1.1339034	244.066667	122.367	121.7
21	2020-09-28 00:00:00	2020-10-19 00:00:00	21	3.66905	0.88364	2.29392	0.65202	1.37513	0.4822155	77.05	48.1722	28.8778
										77.05	48.17	28.87
									Annual_flux(g)	5.96988333	4.29595	1.67392

Data for calcifiers

The data table corresponds to the calcifiers vertical flux in terms of $CaCO_3$. Bottle_no represents the sample number and no_ptero, no_retro and no_foram represents the number of individuals found in the sample of each species/group. ptero_len, retro_len and foram_len corresponds to the average shell size of the individuals. No_days is the duration of the bottle opening. Dw_ptero, dw_LR, DW_foramare the dry weight(s) of each species/group. *L.helicina, L.retroversa* and foraminifer indicate the contribution of each species/group to vertical flux as $CaCO_3$. $CaCO_3$_f is the combined vertical flux of all species/group, followed by monthly_flux of each sample, which is combined to obtain annual vertical flux as Ann_flux.

bottle_n	no_pterc	ptero_le	no_pterc	retro_ler	no_forar	foram_le	no_days	start_date	end_date
1	57	0.58	7	0.74	167	0.14	28	2019-11-18 00:00:00	2019-12-16 00:00:00
2	59	0.68	45	1.05			28	2019-12-16 00:00:00	2020-01-13 00:00:00
3	18	0.76	202	0.97	1	0.15	28	2020-01-13 00:00:00	2020-02-10 00:00:00
5	15	0.82	3	1.03			14	2020-03-09 00:00:00	2020-03-23 00:00:00
7	67	0.87	5	1	17	0.23	14	2020-04-06 00:00:00	2020-04-20 00:00:00
9	70	0.86	1	0.98			7	2020-05-04 00:00:00	2020-05-11 00:00:00
11	4	0.96					7	2020-05-18 00:00:00	2020-05-25 00:00:00
13	10	1.04	2	0.96	1	0.18	14	2020-06-01 00:00:00	2020-06-15 00:00:00
15	47	1.77			23	0.21	14	2020-06-29 00:00:00	2020-07-13 00:00:00
17	5	0.52			1	0.14	14	2020-07-27 00:00:00	2020-08-10 00:00:00
19	416	0.45			5	0.16	14	2020-08-24 00:00:00	2020-09-07 00:00:00
21	30	0.66	0		1	0.13	21	2020-09-28 00:00:00	2020-10-19 00:00:00

DW_pter	DW_LR	DW_Fora	L.helicina	L.retrove	Foramint	pim_mea	CaCO3_f	Monthly_flux
2.6561	0.0001	0.0094	0.8108	4E-05	0.0029	37.114	0.8137	22.78311408
3.4904	0.0021		1.0655	0.0007	0	25.793	1.0661	29.85090062
1.2583	0.0078	7E-05	0.3841	0.0024	2E-05	5.5012	0.3865	10.82199338
1.1752	0.0001		0.7175	8E-05	0	7.5262	0.7175	10.0456854
5.7368	0.0002	0.0028	3.5023	0.0001	0.0017	9.7024	3.5042	49.05862839
5.8906	4E-05		7.1924	5E-05	0	9.1008	7.1925	50.34733828
0.397			0.4848	0	0	14.562	0.4848	3.393271395
1.1192	8E-05	1E-04	0.6833	5E-05	6E-05	11.026	0.6834	9.567232073
11.682		0.0032	7.132	0	0.0019	5.2667	7.134	99.87564324
0.1978		6E-05	0.1207	0	3E-05	1.029	0.1208	1.690896478
13.246		0.0004	8.0867	0	0.0002	13.526	8.0869	113.217011
1.697		5E-05	0.6907	0	2E-05	2.2939	0.6907	14.50506792
								14.505
							Ann_flux	0.429661782

Data for chlorophyll

Bottle_num is the sample number followed by chla_mean, which are the mean values of the triplicates. Chla_sd = chlorophyll a standard deviations, phaeo_n = phaeopigments triplicates mean, phaeo_s = phaeopigments standard deviations and chlaPhaeo_m is the mean values of the triplicates of chl a/phaeopigments. No_days is the duration, for which the bottle was kept open. Last of all, montly flux of each sample (chla_mean*no_days) which is combined as annual(g).

bottle_n	chla_me	chla_sd	phaeo_n	phaeo_s	chlaPhaeo_m	no_days	monthly_flux
1	0.7791	0.0497	5.3617	0.7717	0.14531058	28	21.8149476
2	0.6218	0.1045	4.1221	0.4762	0.15085829	28	17.4117839
3	0.0714	0.0348	0.4413	0.0994	0.16182985	28	1.99979298
4	0.222	0.1064	1.0869	0.2567	0.20425429	28	6.21589181
5	0.6786	0.1386	3.6656	0.2604	0.18513988	14	9.50101968
6	0.2554	0.072	1.324	0.0498	0.19290211	14	3.57561131
7	0.2286	0.0362	0.7297	0.0621	0.31324244	14	3.19999639
8	0.1802	0.0178	0.4465	0.1211	0.40355799	14	2.52290921
9	0.3667	0.0056	0.9261	0.5044	0.3959078	7	2.56664139
10	0.2898	0.0951	0.7288	0.3301	0.39760226	7	2.02845697
11	1.0462	0.9375	0.7265	0.3942	1.44002562	7	7.32306633
12	0.4487	0.0675	1.6021	0.1045	0.28004558	7	3.1405841
13	0.4052	0.0918	1.6717	0.1773	0.2423613	14	5.67223847
14	0.8066	0.2224	5.2715	0.238	0.15300732	14	11.2920952
15	0.93	0.166	5.8072	1.3212	0.16014468	14	13.0197789
16	0.7712	0.1432	4.234	0.1335	0.18215369	14	10.7973986
17	0.4383	0.042	2.458	0.4997	0.17831513	14	6.13627387
18	0.4438	0.1825	3.4717	0.4194	0.12783532	14	6.21320835
19	0.7708	0.116	5.468	1.3116	0.14096793	14	10.7913964
20	0.3206	0.0178	2.3758	0.0108	0.13492532	21	6.73162055
21	0.2406	0.0297	0.8011	0.1399	0.30035544	21	5.05293608
							5.0529
						annual(g)	0.16206055

Appendix 2

R script for plots

TPM Plot 1

```
plot1 <- ggplot(lt_trap_fluxes_plotTPM, aes(x = mid, fill = name)) +
  xlab(NULL) +
  ylab(expression(TPM ~ flux ~ (mg~m^-2~d^-1))) +
  geom_bar(aes(y = mean), color = "black", stat = "identity", width = lt_trap_fluxes_plotTPM$width) +
  geom_errorbar(data = lt_trap_fluxes_plotTPMerrorbars, aes(mid, ymin = mean - sd, ymax = mean + sd), inherit.aes = FALSE) +
  scale_x_date(labels = date_format("%b"), breaks = date_breaks(width = "1 month"), expand = c(0, 0)) +
  theme_bw() +
  scale_fill_manual(values = c("pim" = "lightgray", "pom" = "darkgray")) +  # Specify fill colors for bars
  facet_grid(space = "free_x") +
  scale_y_continuous(expand = c(0, 0), limits = c(0, 72)) +
  theme(axis.text = element_text(size = 20), axis.title = element_text(size = 22, face = "bold")) +
  theme(legend.position = "none")  # Remove legend for Plot 1
```

TPM Plot 2

```
plot2 <- ggplot(lt_trap_fluxes) +
  xlab(NULL) +
  ylab(NULL) +
  geom_bar(aes(x = mid, y = round(pim_percentage) + round(pom_percentage), fill = "PIM"), color = "black", stat = "identity", width = lt_trap_fluxes$width, position = "stack") +
  geom_bar(aes(x = mid, y = round(pom_percentage), fill = "POM"), color = "black", stat = "identity", width = lt_trap_fluxes$width, position = "stack") +
  scale_x_date(labels = date_format("%b"), breaks = date_breaks(width = "1 month"), expand = c(0, 0)) +
  theme_bw() +
  theme(axis.text = element_text(size = 20), axis.title = element_text(size = 22)) +
  scale_y_continuous(expand = c(0, 0), limits = c(0, 100)) +
  labs(y = "%PIM and %POM to TPM") +
  scale_fill_manual(
    values = c("PIM" = "lightgray", "POM" = "darkgray"),
    name = "TPM")
```

```
# Combine the two plots with a common x-axis and shared legends using patchwork
combined_plot <- plot1 / plot2 + plot_layout(guides = "collect")
# Display the combined plot
combined_plot
```

Chlorophyll script

Plot 1

```
lt_trap_fluxes %>%
  ggplot(aes(x=mid,y=chla_mean))+
  geom_bar(color="black", fill="gray" , stat = "identity", width=lt_trap_fluxes$width)+
  geom_errorbar(aes(ymin=chla_mean-chla_sd,ymax=chla_mean+chla_sd))+
  labs(x="2019-2020",y=expression(Chl~a~flux~(mg~m^-2~d^-1)))+
  scale_x_date(labels=date_format("%b"),
               breaks = date_breaks(width = "1 month"),
               expand = c(0,0))+
  theme_bw()+
  theme(axis.text=element_text(size=20),
        axis.title=element_text(size=22))
phaeo <- lt_trap_fluxes$chlaPhaeo_mean
```

chl:phaeo

```
chl_phaeo_ratio <- lt_trap_fluxes %>%
  ggplot(aes(x = mid, y = chlaPhaeo_mean)) +
  geom_bar(color = "black", fill = "gray", stat = "identity", width = lt_trap_fluxes$width) +
  labs(x = "2019-2020", y = "Chl-a/Phaeo-pigments") +
  scale_x_date(labels = date_format("%b"), breaks = date_breaks(width = "1 month"), expand = c(0, 0)) +
  theme_bw() +
  theme(axis.text = element_text(size = 20), axis.title = element_text(size = 24))
chl_phaeo_ratio
phaeo <- lt_trap_fluxes$chlaPhaeo_mean
chl_phaeo_ratio  # Display the plot
```

Calcifiers script

Plot 1

```
#1 Create a scatter plot with separate lines for each set of data
ggplot(Calcifiers_flux_plot, aes(x = as.Date(start_date))) +
```

```
  geom_point(aes(y = ptero_length, color = "L.helicina"), size = 4) +
  geom_line(aes(y = ptero_length, group = 1), color = "black", na.rm = FALSE, size = 0.5) +
  geom_point(aes(y = retro_length, color = "L.retroversa"), size = 4) +
  geom_line(aes(y = retro_length, group = 2), color = "brown", na.rm = FALSE, size = 0.5) +
  geom_point(aes(y = foram_length, color = "Foraminifers"), size = 4) +
  geom_line(aes(y = foram_length, group = 3), color = "darkgray", na.rm = FALSE, size = 0.5) +
  scale_x_date(labels = scales::date_format("%b"), breaks = scales::date_breaks("1 month")) +
  labs(x = "2019-2020", y = "Mean length(mm)") +
  theme_minimal() +
  scale_color_manual(values = c("L.helicina" = "black", "L.retroversa" = "brown", "Foraminifers" = "darkgray")) +
    theme(legend.title = element_blank(),
        legend.position = "top",legend.text = element_text(size =20),
        axis.text = element_text(size = 16),
        axis.title = element_text(size = 20),
        plot.title = element_text(size = 16, hjust = 0.5)) +
  scale_y_continuous(expand = c(0, 0), limits = c(0.0, 1.8), breaks = seq(0.0, 1.8, by = 0.2))
```

Plot 2

```
bar_plot1 <- ggplot(Calcifiers_organism_normal, aes(x = as.Date(start_date), y = lim_h_no)) +
  geom_bar(stat = "identity", color = "black", fill = "gray", width = 15, na.rm = FALSE) +
  scale_x_date(labels = scales::date_format("%b"), breaks = scales::date_breaks("1 month")) +
  labs(x = NULL, y = "Limacina helicina flux ind~m^-2~d^-1") +
  theme_minimal()
bar_plot2 <- ggplot(Calcifiers_organism_normal, aes(x = as.Date(start_date), y = lim_r_no)) +
  geom_bar(stat = "identity", color = "black", fill = "gray", width = 15, na.rm = FALSE) +
  scale_x_date(labels = scales::date_format("%b"), breaks = scales::date_breaks("1 month")) +
  labs(x = NULL, y = "Limacina retroversa flux ind~m^-2~d^-1") +
  theme_minimal() +
  theme(axis.title.x = element_blank())
bar_plot3 <- ggplot(Calcifiers_organism_normal, aes(x = as.Date(start_date), y = foramini_no)) +
  geom_bar(stat = "identity", color = "black", fill = "gray", width = 15, na.rm = FALSE) +
  scale_x_date(labels = scales::date_format("%b"), breaks = scales::date_breaks("1 month")) +
  labs(x = "2019-2020", y = "Foraminifers flux ind~m^-2~d^-1") +
  theme_minimal()
```

```
# Combine the plots into one
combined_plot <- cowplot::plot_grid(bar_plot1, bar_plot2, bar_plot3, ncol = 1, align = "v")
# Display the combined plot
print(combined_plot)
```

Plot 3

```
bar_plot <- ggplot(Calcifiers_flux_plot, aes(x = as.Date(start_date))) +
  geom_bar(aes(y = CaCO3_flux), stat = "identity", color = "black", fill = "gray", width = 15) +
  scale_x_date(labels = scales::date_format("%b"), breaks = scales::date_breaks("1 month")) +
  labs(x = "2019-2020", y = "CaCO3 flux mg m-²d-1") +
  theme_minimal() +
  theme(
    axis.text = element_text(size = 14),            # Adjust axis text size
    axis.title = element_text(size = 18),           # Adjust axis title size
    plot.title = element_text(size = 16, hjust = 0.5) # Adjust plot title size
  )
# Display the bar plot
print(bar_plot)
```

Plot 4

```
ggplot(Calcifiers_flux_plot) +
  xlab("2019-2020") +
  ylab("Percentage") +
  geom_bar(aes(x = as.Date(start_date), y = round(percent_CaCO3) + round(PIM_excl_CaCO3), fill = "PIM excluding CaCO3"), color = "black", stat = "identity", width = Calcifiers_flux_plot$no_days, position = "stack") +
  geom_bar(aes(x = as.Date(start_date), y = round(percent_CaCO3), fill = "CaCO3"), color = "black", stat = "identity", width = Calcifiers_flux_plot$no_days, position = "stack") +
  scale_x_date(labels = date_format("%b"), breaks = date_breaks(width = "1 month"), expand = c(0, 0)) +
  theme_bw() +
  theme(axis.text = element_text(size = 20),
        axis.title = element_text(size = 22,)) +
  scale_y_continuous(expand = c(0, 0), limits = c(0, 100)) +
  labs(y = "%CaCO3 and % PIM excluding CaCO3") +
  scale_fill_manual(
    values = c("PIM excluding CaCO3" = "lightgray", "CaCO3" = "darkgray"))+theme(legend.title = element_blank(),
                                                                                 legend.position = "top")
```